Engineering Geology 219 (2017) 32–51

Contents lists available at ScienceDirect

Engineering Geology

journal homepage: www.elsevier.com/locate/enggeo

Application of geotechnical and geophysical field measurements in an active alpine environment

D.R. Lucas *, K. Fankhauser, S.M. Springman

ETH Zürich, Institute for Geotechnical Engineering, Wolfgang-Pauli-Str. 15, 8093 Zürich, Switzerland

ARTICLE INFO

Article history:
Received 1 April 2016
Received in revised form 23 September 2016
Accepted 21 November 2016
Available online 24 November 2016

ABSTRACT

A gravelly scree slope in the Meretschibach catchment, a location in the Swiss Alps in the vicinity of Agarn, canton Valais, has been observed to deform downslope at up to 0.5 m p.a. The potential instabilities at this site include surficial landslides, some of them originally thought to be triggered by an increase in pore water pressure with a subsequent loss of shear strength as a consequence of rainfall infiltration and rockfalls. A programme consisting of monitoring, laboratory testing and investigation was developed, to perform a thorough soil characterisation needed in order to produce a realistic ground model. The long-term geotechnical monitoring included in situ soil temperature, suction as well as volumetric water content measurements using dielectric permittivity and time domain reflectometry (TDR) sensors. This data was complemented by electrical resistivity tomography (ERT) to provide extensive knowledge on the depth to bedrock and to validate the volumetric water contents in specific locations. The datasets are completed by recordings from two nearby weather stations. Seasonal changes of precipitation and temperature were reflected in corresponding trends in all measurements. A comparison of volumetric water content records was obtained using capacitance and time domain reflectometry (TDR) sensors with ERT, yielding reasonable agreement. The resulting ground model, which integrates all currently available parameters, delivers the essential information and boundary conditions for predicting and validating slope instabilities in the future, using numerical and physical modelling.

1. Introduction

The Meretschibach catchment (Fig. 1), situated in the Swiss Alps, canton Valais, near the village of Agarn (620 m.a.s.l.), has been investigated due to dynamic processes of erosion, deposition and remobilisation of debris, which can evolve into different kinds of mass movement. Debris flows have reached Agarn from an active channel and caused damage to infrastructure in the past. This has been well documented (Rickenmann and Zimmermann, 1993; Oggier, 2011). However, little has been published about slope instabilities triggered in gravelly soils in the adjacent scree slope, where surface movements of up to 0.5 m p.a. have been obtained from InSAR measurements (Dr. Hugo Raetzo, 2012, FOEN, pers. Comm.).

Three prevalent types of downslope movement were expected, either based on past research (Springman et al., 2012), or observed during the monitoring programme on the steep scree slope:

- shallow landslides triggered by an increase in pore water pressure that reduces soil suction and shear strength;
- boulders that topple, fragment, bounce and roll downslope from weathered rock walls at the top of the slope;
- ongoing surficial erosion, including destabilisation of the top ground layer through rainfall runoff and flow, movement of dry debris as well as small avalanches in winter.

Characterisation and long-term monitoring of this slope are necessary in order to gain more understanding of these processes, although this is complicated by slope inclinations of 33–43°, heterogeneous gravelly soil, patches of native vegetation, seasonal limitations and difficult accessibility due to the alpine location at 1840–2000 m.a.s.l. A realistic ground model can be established, defining extent of soil layers and depth to bedrock, as well determining relevant soil properties at different depths.

A long-term monitoring campaign, integrating geotechnical and geophysical methods together with laboratory analyses, allows a progressively more detailed calibration and validation of the ground model and relevant parameters, while observing and measuring the response of the scree slope to seasonal processes. Instrumentation was installed in the scree slope at shallow depths (<1 m) within four trenches (IT1-IT4), to perform real time monitoring of the volumetric water content (VWC), temperature and suction (Lucas et al., 2015; Springman et al., 2015). The VWC and the suction measurements

* Corresponding author.
E-mail addresses: daisy.lucas@igt.baug.ethz.ch (D.R. Lucas), kerstin.fankhauser@igt.baug.ethz.ch (K. Fankhauser), sarah.springman@igt.baug.ethz.ch (S.M. Springman).

http://dx.doi.org/10.1016/j.enggeo.2016.11.018

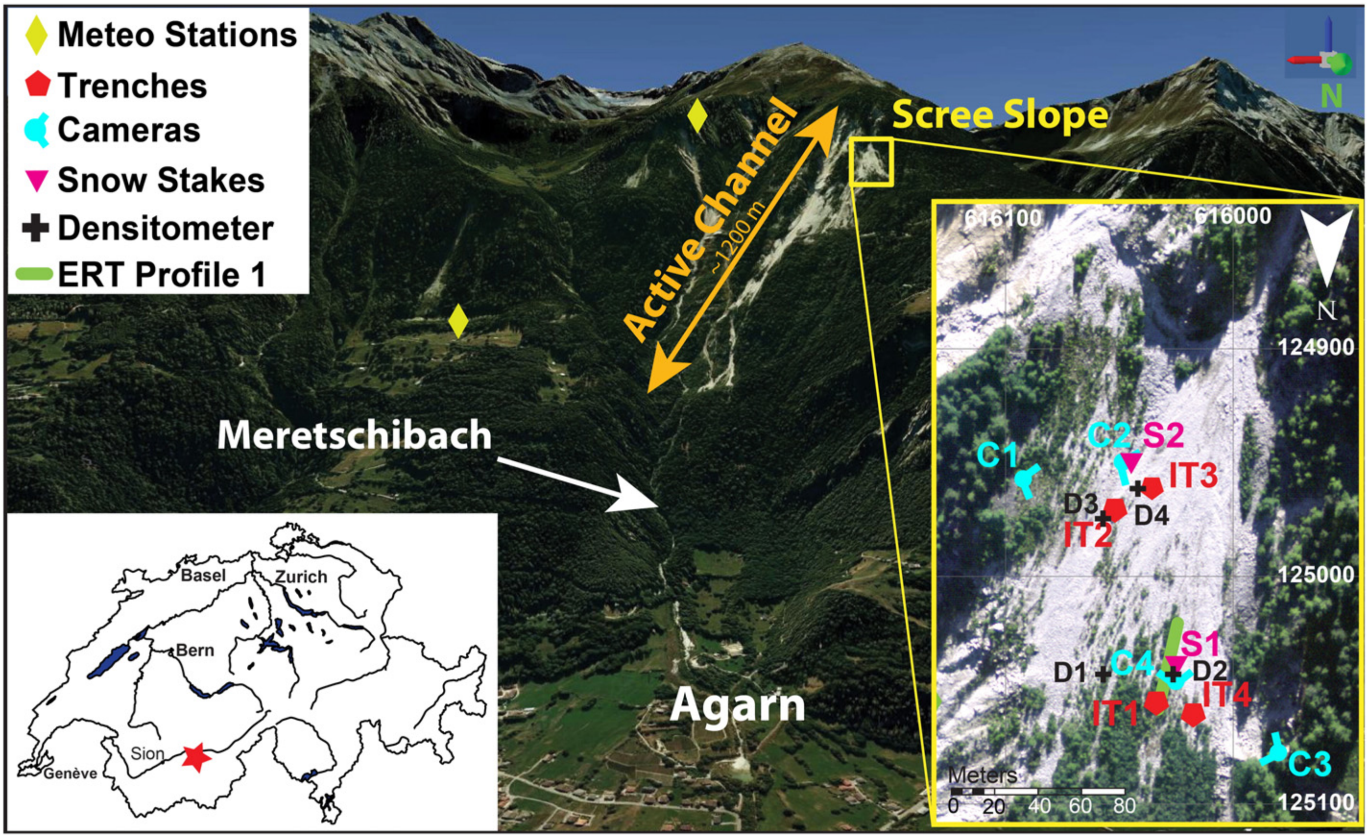

Fig. 1. Overview of the field area, located in canton Valais, Switzerland (star on small map). The image looking south shows a view of Agarn, situated on the Rhone valley floor and the Meretschibach catchment on the mountain slopes behind. The most active area within the catchment can be divided into an active channel and a scree slope. The weather stations (yellow diamonds) are located at 1370 m.a.s.l. (IGT) and 2220 m.a.s.l. (WSL). The right image shows an enlargement of the scree slope (yellow rectangle) with the locations of the instrumented trenches (IT1-IT4), the ERT profile on which the monitoring was performed, snow stakes (S1–S2), densitometer measurements (D1–D4) and cameras (C1–C4).

provide valuable information to assess changes in soil shear resistance, particularly for soil in a partially saturated state and to enable a comparison between the VWC acquired by two different types of moisture sensors. Additionally, the precipitation in the area was measured with two weather stations located within a distance of 2 km, at elevations of 2220 and of 1370 m.a.s.l., respectively.

Geophysical measurements complemented the long term soil monitoring, providing a convenient way to extend the knowledge of the subsurface to larger areas in the scree slope (Bogoslovsky and Ogilvy, 1977; Hack, 2000; Bichler et al., 2004; Otto and Sass, 2006; Sass, 2007; Sass et al., 2008). Electrical resistivity tomography (ERT) measurements were conducted repeatedly throughout the spring and summer months of 2014, on a profile located close to IT1 (Fankhauser, 2014), allowing the in situ VWC recordings to be validated in specific locations using Archie's law (Archie, 1942; Friedel et al., 2006). Effective validation can demonstrate complementarity of geotechnical and geophysical methods and provide a more widespread interpretation of the volumetric water content (VWC), leading to a more detailed characterisation of the scree slope.

The data presented here was acquired over a period of two years, and is analysed by seasons. Trends in summer and winter, and thawing/freezing processes in spring and autumn, are discussed further.

2. Soil ground characteristics

2.1. Soil classification

Fig. 1 shows the location of the research site and, specifically, the instrumented trench sites IT1–IT4. Samples were taken from test pits and trenches during dry summer weather conditions. The following characteristics were noted: the ground surface was considered to be 'depth zero' for each test pit; at least 4 kg of soil were extracted for each disturbed sample. Cobbles larger than 70 mm, and any boulders, were left at the site. Roots were found in almost all of the samples.

Grain size analyses were performed later in the laboratory. The soil is mostly gravel, with diverse percentages of sand and fines, and it is classified (Figs. 2, 3 and Table 1) according to Swiss standard classification (SN 670004-2NA), as poorly-graded gravel with silt and sand (GP-GM), silty gravel (GM), well-graded gravel with silt and sand (GW-GM), and well-graded gravel (GW). Fig. 2 shows the soil profiles in the instrumented trenches.

Three common soil units are found in IT1, IT2 and IT4, but with different thicknesses: (A) gravel with fines and high root content; (B) gravel with fines, and less or no roots, (C) coarser gravel. An orange dashed line separates the gravel from a soil layer with greater fines content, considered here as more stable and suitable for instrumentation placement, from either coarser gravel layers or isolated lenses of coarser gravel that were more unstable for excavation (IT4). In contrast, IT3 consists of two different units described as finer gravel (D) and a transition to slightly coarser gravel (E).

2.2. In situ unit weight

The in situ unit weight was determined with a soil densitometer (Magdeburger Prüfgeräte GmbH (HMP)), which uses the balloon method (DIN 18125-2:2011-03) from which void ratio and porosity can be derived. It could be transported to alpine sites to carry out measurements in gravelly soil.

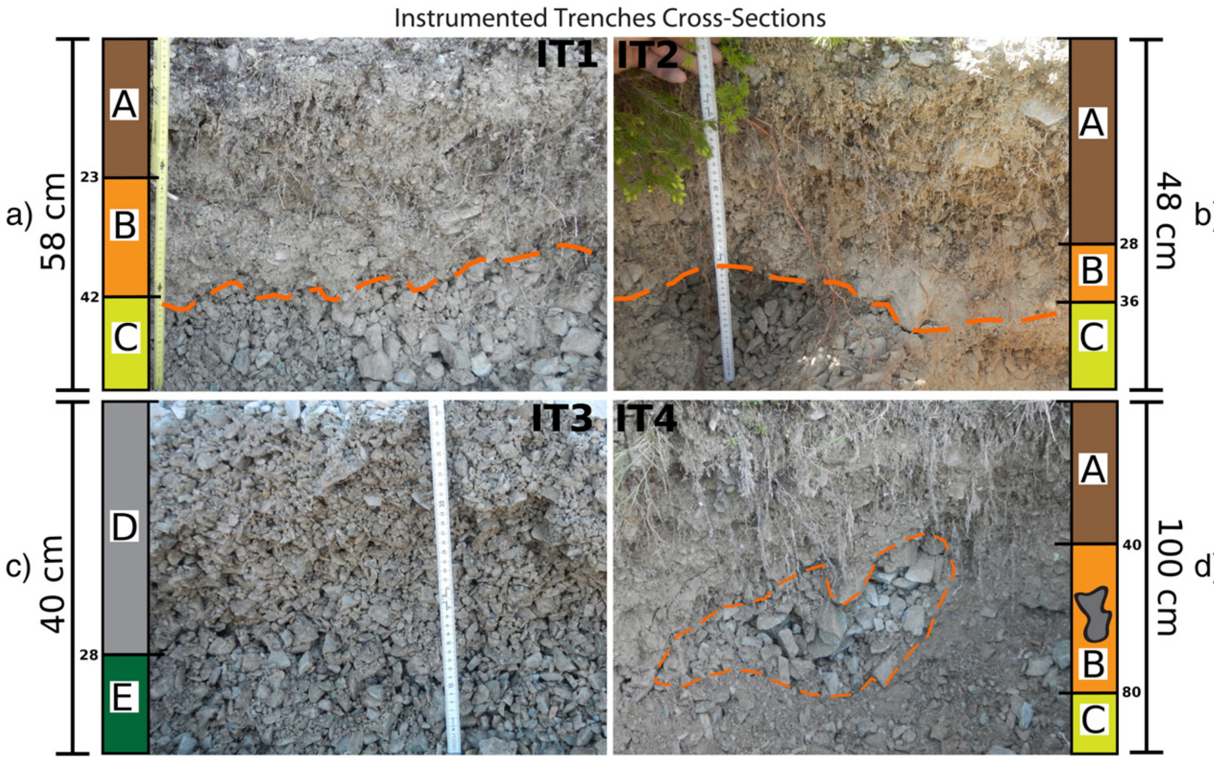

Fig. 2. Soil profiles at instrumented trenches. a) IT1, b) IT2, c) IT3 and d) IT4. For IT1, IT2 and IT4: A (depth ~0–40 cm), gravel with silt, sand and some roots; B (depth ~25–40 cm), gravel with silt and sand; C (depth below ~40 cm), coarser gravel with less fines; IT3: D (depth ~0–25 cm), gravelly soil with little sand and silt content; E (depth below ~25 cm) change to a coarser gravel.

The unit weights calculated from the tests are presented in Table 2 and the test locations are shown in Fig. 1. These values were in agreement with the void ratio range of 0.34–0.69, which was determined in the laboratory from test samples.

2.3. Slope inclination

The slope inclination in the scree slope (Fig. 4) was obtained using the geographical information system (GIS). The most predominant angle of inclination in the scree slope is between 33 and 43°, although some steeper areas (mostly upslope) can be identified > 43°.

2.4. Instrumented trenches

Selected spots on the scree slope (i.e. landslide source areas) are monitored in situ to measure water infiltration-suction characteristics in the ground, to provide time-series data on infiltration quantities and rates, as well as the influence on the capillary suction, which

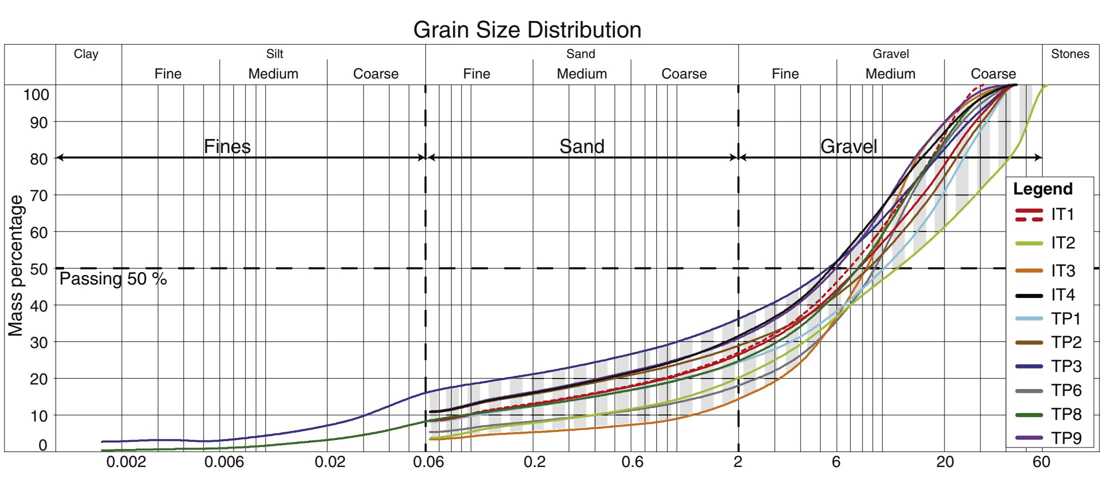

Fig. 3. Grain size distribution: a selection from Meretschibach scree slope test pits TP 1–9 are plotted, together with IT1–IT4. The range is shaded in grey to illustrate the characteristics and content of fines for the entire set of samples.

Table 1
Soil classification from test pits and instrumented trenches.

Test pit	Swiss standard classification (SN 670004-2b NA)	Moisture content [%]	Percent of fines [%]	C_u [−]	C_c [−]	G_S [−]
TP1	GP-GM	2.9–3.7	5.7–8.2	73.6–139.3	8.3–14.4	
TP2	GP-GM	3.0–5.4	5.5–10.8	33.3–105.1	7.9–11.2	
TP3	GM	3.7–4.3	6.7–16.4	72.8	9.1	
TP4/IT1	GP-GM	–	7.7–9,2	98.2–115.3	6.2–8.2	2.68
TP5	GP-GM	–	5.7	37.6	5.0	
TP6	GP-GM	–	5.4	28.7	5.1	
TP7	GP-GM	–	8.4	106.1	7.7	
TP8	GP-GM	–	8.5	110.2	10.1	
TP9		–	11.0	–	–	
TP10	GW-GM		11.7	94.9	2.2	
IT2	GW	2.2	4.0	46.9	2.32	
IT3	GW		3.4	8.4	1.9	
IT4	GP-GM		10.9	47.5	2.32	

C_u: Coefficient of uniformity, C_c: Coefficient of curvature; G_S: Specific gravity.

directly affects the effective stress. Four monitoring profiles were installed (IT1–IT4, Figs. 1 and 2), consisting of sets of dielectric permittivity sensors (EC-5 and 10HS), time domain reflectometry (TDR) soil moisture and temperature sensors (Table 3). Two trenches, IT1 and IT4, are supplemented by co-located tensiometers. All of the sensors were installed in trenches up to 1 m depth and of minimum 1 m width, to minimise interference between sensors at similar depths.

Two weather stations were installed and are monitored within the study area, a SR50A Campbell weather station (precipitation, ambient air temperature, humidity) controlled by the Swiss Federal Institute for Forests, Snow and Landscape research (WSL), and an OTT Pluvio^2 device (precipitation, ambient air temperature, humidity and wind direction) installed by ETH (IGT). While the Campbell station is used to measure precipitation in the form of rain when the ambient air temperature is higher than zero (no heater), the OTT Pluvio^2 is able to measure precipitation in the form of rain, snow, or a mixture of both during all seasons.

Environmental changes, including freezing/thawing conditions, particularly during the crucial autumn/spring snow-melt period, can be identified through ambient and soil temperature measurements. The TDRs and dielectric permittivity sensors (EC-5, 10HS) are calibrated to measure the volumetric water content (VWC).

2.4.1. Sensors and calibration

2.4.1.1. Sensors. Two types of sensor were installed to measure VWC (Table 3): time domain reflectometry (TDR100; Campbell Scientific) and capacitance sensors (EC-5 and 10HS; Decagon Devices), via the apparent dielectric constant/permittivity of the soil surrounding the probes.

The volume of sensitivity of the sensors (soil volume influenced during VWC measurement) becomes relevant while interpreting data in terms of first response to a saturation event. A representative VWC of gravel in the scree slope should reflect the range of particle sizes and the measurement volumes, with 181 (Onset, n.d.) and 1160 cm^3 (ICT international, 2008) respectively for EC-5s and 10HSs (method after Sakaki et al., 2008), and 1.4 times the diameter of the rod spacing (2.1 cm) for TDRs (O'Connor and Dowding, 1999), leading to a volume of 101 cm^3 (Table 3).

The suction was recorded with tensiometers (Jetfill 2725 in IT1 and Remote 2100F in IT4; Keller AG), paused in October before winter (to avoid freezing conditions) and restarted again in May. While the Jetfill were installed a few metres upslope of the trench, to a maximum depth of 0.45 m, the Remote were installed in the trench with the other instruments at different depths (up to 1 m).

Further information on all sensors can be found in supplementary material A.

Table 2
Dry unit weight obtained with the soil densitometer method.

Measurement	Dry unit weight [kN/m^3]	Void ratio [−]	Relative density [%]	Porosity [−]
D1	17.63	0.52	48.57	0.34
D2	16.98	0.58	31.43	0.37
D3	17.69	0.51	51.43	0.34
D4	16.09	0.66	8.57	0.40

2.4.1.2. Calibration. The capacitance and TDR sensors were calibrated in the laboratory using poorly-graded gravel with silt and sand (GP-GM) from the field, over the range of VWCs estimated for the unsaturated conditions expected in situ. The specimens were prepared by moist tamping, with void ratios in the range of $e = 0.53 - 0.69$, simulating suitable installation conditions with both medium and loose densities.

A linear calibration was fitted to the measured values in most cases, in which the coefficient of determination was $r^2 = 0.56–0.98$. In some cases, this could be improved by fitting a polynomial equation, and this was adopted, for instance, for IT2 capacitance sensor 10HS at 13 cm depth.

Although Topp's equation (Topp et al., 1980) allows prediction of VWC for grain sizes up to 2 mm, the VWC obtained were between factors of 2–3 smaller than for a site-specific linear calibration at 20 °C using the soil from the field with a $d_{max} \leq 31.5$ mm (albeit with a 8% content of fines). This significant difference could be due to effect of the texture, structure, and density on the electrical response in soils, as mentioned by Topp et al. (1980). These results confirm that a site specific calibration function is necessary when using poorly-graded gravel with silt and sand. While Topp's approach could not be completely applicable to the grain size distribution of the scree slope, the adjustment of the permittivity due to changes in temperature derived by Bogena et al. (2007), using a liquid with known dielectric properties (2-isopropoxyethanol (i-C3E1) water mixtures) was tested against Bogena's equation for loamy silt. This has a significant effect on the calculated VWC, which in many cases maps closely to the values of the site-specific calibration results. As the use of a site-specific calibration function has been recommended by other authors (e.g. Take et al., 2007 and Mittelbach et al., 2011), this has been adopted. A site-specific equation for the correction of permittivity due to temperature (applicable to capacitance sensors installed in scree soil) is advised for future studies.

Ultimately, the performance of a sensor type is directly related to the soil conditions in the field. Large stones and boulders, sometimes comparable to the size of the capacitance sensor prongs, complicate effective insertion of the probes into the soil. Heterogeneity contributes natural variability in density, void ratio and grain sizes that have impacted on the process of site-specific calibration and functionality of TDRs and capacitance sensors during monitoring.

2.5. Electrical resistivity tomography (ERT)

A 2D electrical resistivity survey was carried out on a fixed profile line next to instrumented trench IT1 (Fig. 1) to complement the point measurements from the TDRs and dielectric permittivity sensors, and achieving a more widespread characterisation of the subsurface. The basic principle of geoelectrical resistivity measurements, as well as the equipment and configurations used in this project, are briefly summarised in Supplementary material A. Further details on acquisition, processing etc. can be found in Fankhauser (2014), Günther and Rücker (2013), Günther et al. (2006), Günther (2011), Rücker et al. (2006) and Lowrie (2007). A total of six ERT measurements (three of which are presented here) were poorly-graded gravel with silt and sand (GP-GM) conducted in a monitoring phase from May to July 2014.

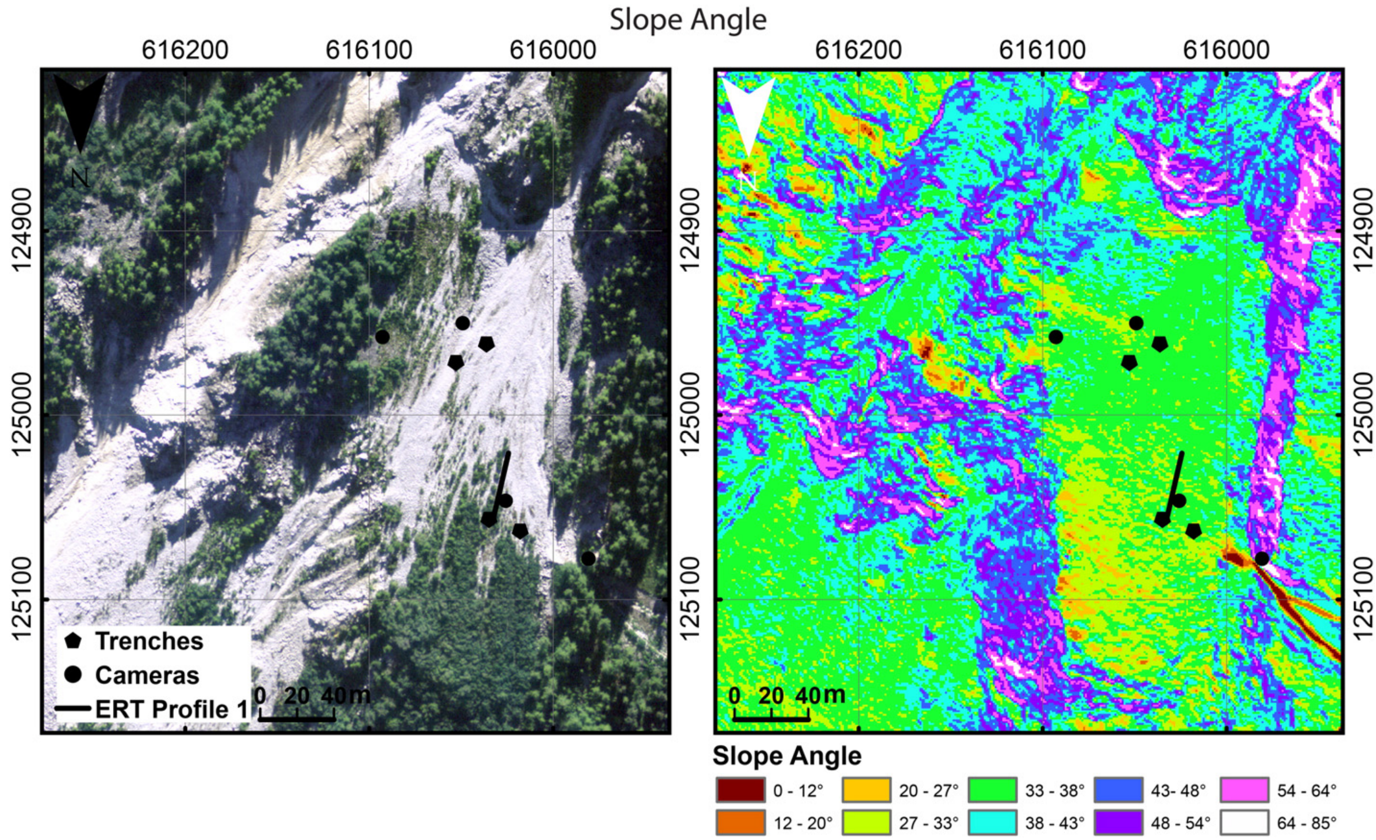

Fig. 4. Left: Aerial photograph (SWISSIMAGE) of the scree slope and top part of the active channel; right: slope angle in °: of the same area. Black symbols show the location of instrumentation (see Fig. 1 for comparison).

2.6. Archie's law

ERT measurements are highly susceptible to changes in the subsurface water content/saturation as the current injected during a geoelectrical survey flows mostly through the pore water. An empirical relationship between the resistivity of a porous medium to the amount of pores, their connectivity and saturation, as well as the resistivity of the pore filling fluids, was found by Archie (1942):

$$\rho = a\rho_w \Phi^{-m} S^{-n} \qquad \text{with} \quad S = \frac{\theta}{\Phi} \tag{1}$$

where ρ is the resistivity of the porous soil, ρ_w is the resistivity of the pore filling fluid, Φ is the soil porosity (typically n in a geotechnical context) and S the saturation, which can also be expressed as the ratio between the volumetric water content θ and the porosity. Furthermore, a is the tortuosity factor set to 1 for granular soils, m is the cementation factor and n is the coefficient of saturation. The latter two factors are assumed to be constant and, if taken from literature (e.g. Archie, 1942; Lowrie, 2007; Schön, 1983), are usually given as $m \cong 1.3$ and $n \cong 2$ for granular soil. Archie's law is considered to be valid in this case (without the need for any correction factors), as the soil consists mainly of gravel

Table 3
Technical information about the sensors installed.

Sensor	Name	Brand	Length	Measuring range	Volume of influence cm^3	Accuracy	Temperature range [°C]
Capacitance	EC-5	Decagon Devices[*]	0.089 m	0–100% VWC	240	±1–2% VWC with soil specific calibration	−40 to +50
	10 HS (only IT2)		0.145 m	0–57% VWC with polynomial	1320	using soil specific calibration, ±0.02 m^3/m^3 (±2% VWC) in any soil	Survival temperature: −40–50 Operating temperature: 0–50
Time domain reflectometry	TDR100	Campbell Scientific[**]	0.15 m	0–100% VWC	188.5	±1.5% VWC	−40 to +55
Tensiometers	Jetfill 2725 ARL	Keller AG Company[***]	0.15, 0.30, 0.45 m	0–85 kPa	Direct contact	±1.5%	Avoid freezing conditions
	Remote 2100F	Keller PR23-S[****]	Installed at depths from 0.2 to 1 m.	0–85 kPa			
Temperature	RTD PT100	Heraeus	Installed at depths from 0.2 to 1 m.–	−50 to 100 °C	Direct contact	±0.05 °C	−50 to 100 °C

* http://manuals.decagon.com/Manuals/13876_EC-5_Web.pdf.
** https://s.campbellsci.com/documents/us/manuals/tdr100.pdf.
*** http://www.soilmoisture.com/RESOURCE_INSTRUCTIONS-all_products/Resource_Instructions_0898-2725_2725%20Jet-Fill%20Tensiometers.pdf.
**** http://www.soilmoisture.com/RESOURCE_INSTRUCTIONS-all_products/Resource_Instructions_0898-2100_2100F%20Soilmoisture%20Probe.pdf.

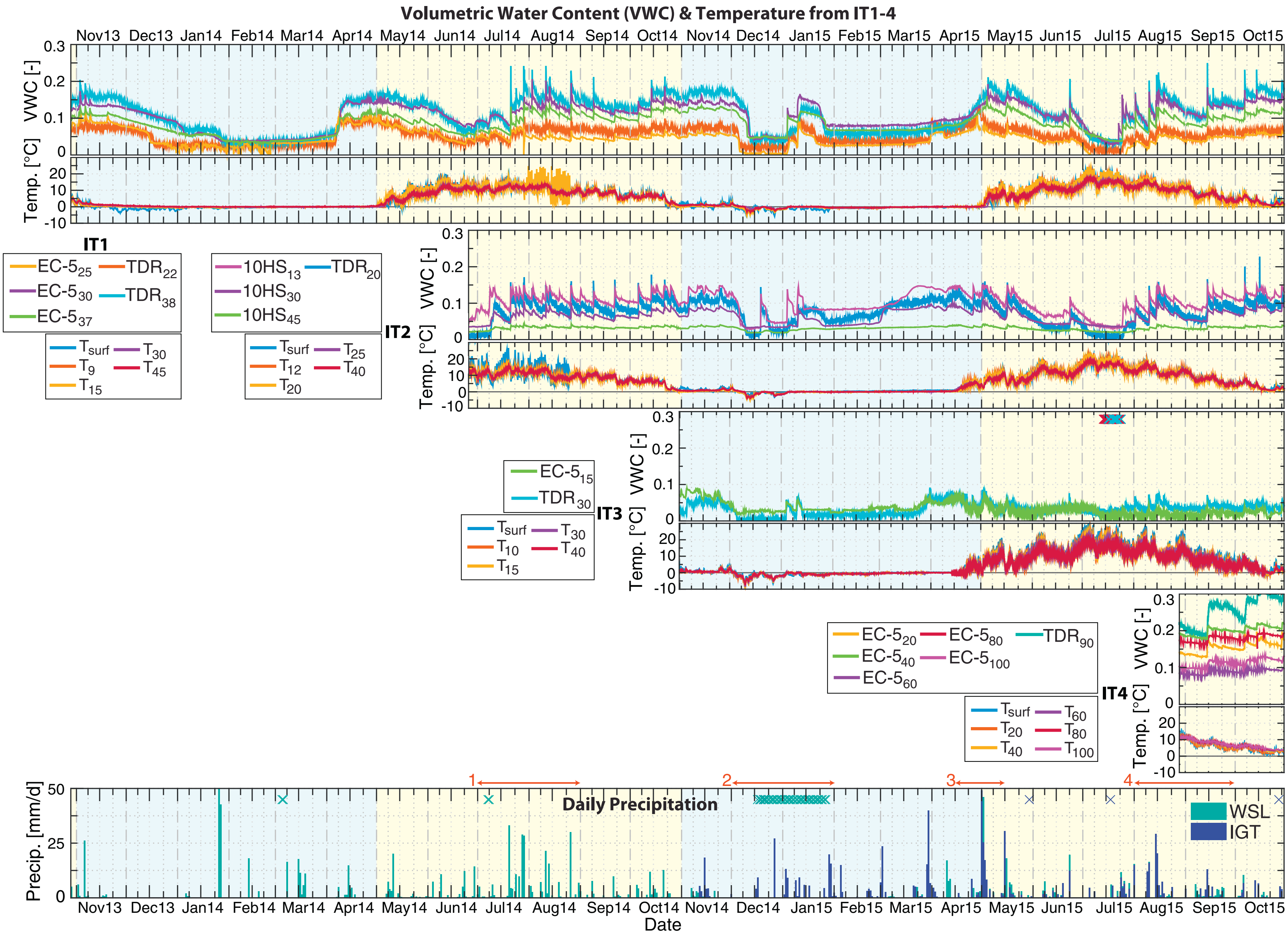

Fig. 5. Overview of measurements at instrumented trenches. From top to bottom for each trench IT1–IT4: VWC, temperature; precipitation from WSL and IGT stations on the bottom.

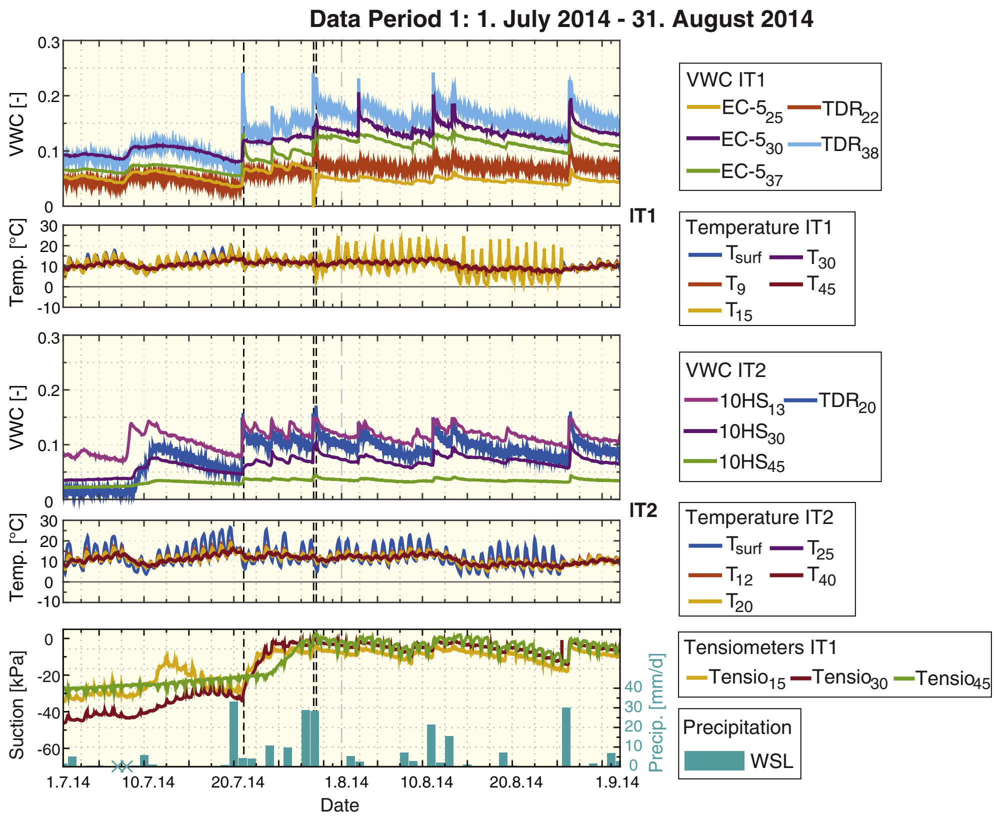

Fig. 6. VWC, temperature and precipitation at IT1–IT2 and suction data at IT1 are displayed from 1st July 2014 to 31st August 2014. The debris flow events in the active channel (Fig. 1) are marked with a dashed line each. The sub-index in the legend indicates the sensor depth in cm. Missing precipitation data are marked with a cross.

and sand and contains almost no fines, especially no clay (Figs. 2 and 3, Table 1). The relationship can be used for effective comparisons between the geotechnical soil moisture measurements and ERT acquisitions (e.g. Brunet et al., 2010; Lehmann et al., 2013; Springman et al., 2013). For this purpose, the key parameters, Φ and ρ_w, were estimated from soil and water samples (small creeks and surface run-off near to the scree slope) extracted from the field, and analysed through laboratory and field experiments as $\Phi = 0.33 \mp 0.08$ and $\rho_w = 155 \mp 28$ Ωm (at 25 °C; for temperature corrections, the equation and the geophysical temperature compensation factor stated in Hayashi (2004) were used).

A convenient way to use the temporally varying soil resistivities (repeatedly measured ERT profile) is to calculate the saturation relative to a so-called baseline model (chosen here as the acquisition on 15th May 2014) and so avoid having to estimate many (uncertain) parameters in Archie's law. The resulting trend (Fig. 16) can be compared relative to the readings obtained from TDR and dielectric permittivity sensors. This process is further described in Supplementary material A.

3. Results and discussion

3.1. VWC and temperature monitoring in instrumented trenches IT1–IT4

An overview of the data time series recorded since October 2013 is presented in Fig. 5, where a set of two plots display the volumetric water content (VWC) and temperature versus time (in months at the bottom and the top, separated by dashed lines), in chronological order of installation for each of the instrumented trenches (from top to bottom: IT1–IT4).

The VWCs displayed in all of the plots range from 0 to 0.3 and the temperatures from −10 to 30 °C. The precipitation from the two weather stations (WSL and IGT) is shown at the bottom, over a range of 0 to 50 mm per day. Each coloured line represents a sensor installed at a given depth, as shown in each legend with the corresponding sensor name (Dec = dielectric permittivity sensor; T = temperature), as well as the depth (in centimetres below the surface) as a sub-index. The VWC from the three types of moisture sensors (dielectric permittivity sensors and TDRs) can be compared when they are at similar depths. T_{surf} is the temperature measured in the data logger at the surface, usually a few metres away from the trench. The background shading represents a definition of summer (yellow) and winter (blue), as the season during which fieldwork can be carried out and a time during which access to the site is not possible, respectively. Missing data due to loss of signals or eliminated data from a specific device are marked at the top of the plot by a cross of the same colour.

Clear and expected seasonal differences are observed between summer, winter and spring/autumn in terms of temperature and volumetric water content (VWC).

3.2. Seasonal response of the scree slope

3.2.1. Summer

Figs. 6 and 7 represent the summers of 2014 and 2015, respectively at different locations of the scree slope (Fig. 1, IT1–IT3). High temperatures in summer, combined with precipitation in the form of rainfall, which infiltrates into the ground, produces almost immediate increases in VWC near the surface. The variation in magnitude of VWC between trenches IT1–3 (Fig. 7) can be attributed to the different grain size distributions (GW: IT2–3; GP-GM: IT1,4). Two types of infiltration behaviour can be identified in trenches IT1-IT2, which can be seen when comparing the VWC in July 2014. The increase of VWC can either be gradual with a convex drop-off as the ground drains, or reach immediate peaks, followed by linear to concave decreases. The former were associated with periods of high suctions (especially in deeper tensiometers, and during periods

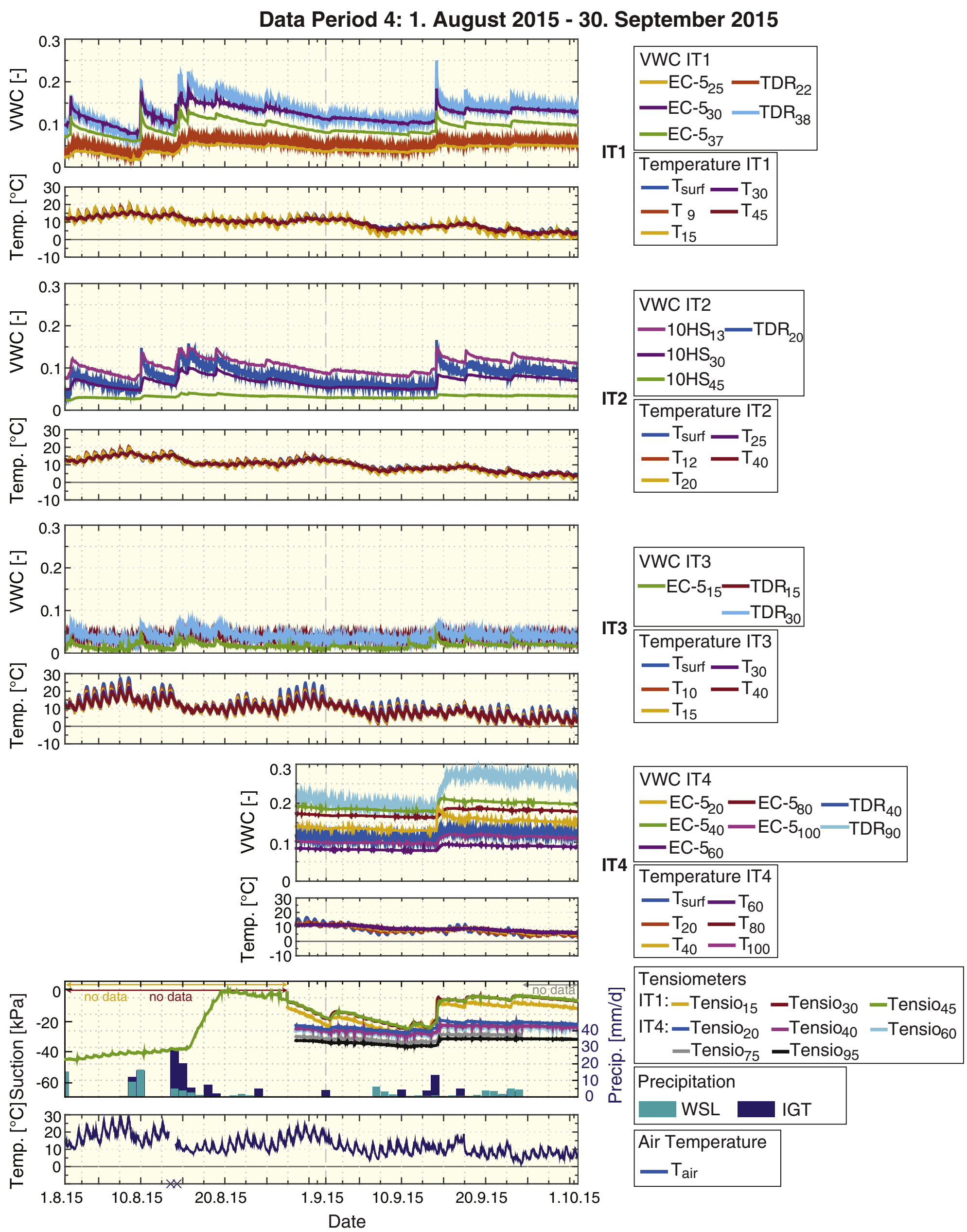

Fig. 7. VWC, temperature and precipitation at IT1–IT4 and suction data from IT1 and IT4 are displayed from 1st August 2015 to 30th September 2015. In addition, the ambient air temperature recorded at the IGT weather station is shown on the bottom. The sub-index in the legend indicates the sensor depth in cm. Missing suction data are marked with an arrow in corresponding colour and missing air temperatures with crosses.

of little to no rainfall), when the unsaturated hydraulic conductivity decreased, while immediate peaks occurs at higher degree of saturation. Furthermore, suctions reduced either in the same timeframe as the rain infiltration or marginally slower than the VWCs had increased. This is due to the radius of influence of the sensors, EC-5 has a greater radius of 20 mm and the tensiometers around 1 mm, therefore capacitance sensors react faster during infiltration (Beck, 2010). Sun exposure is higher in IT3, with temperature ranging from 0 to 27 °C, and daily peaks close to ambient air temperature.

3.2.2. Winter

Temperatures are near or below 0 °C (Fig. 8), so that precipitation occurs in the form of snowfall or mixed with rainfall. The pore water fluid is expected to freeze when temperatures are below 0 °C, decreasing the permeability of the unsaturated soil even further. Snow can accumulate on, and insulate, the slope, reducing the rate and volume of water infiltration (Fig. 8, camera 2, 28.12.2014, 10:00). These two processes explain the degree of saturation dropping to a minimum and the lack of variation in VWC with ongoing winter precipitation (Fig. 8, December, beginning January), while infiltrating precipitation and snow-melt processes cause rising VWC when there is an increase from negative to positive temperatures (Fig. 8, end December, beginning January). Episodes of freezing and snow melting are observed later in some trenches, because the ground temperature is dependent on sun exposure, which differs depending on the location on the scree slope (up- or downslope).

Patterson and Smith (1981) proposed that K_a is not highly sensitive to ice content in partially saturated coarse sand samples, since the slight increment measured is a product of replacing air ($K_a = 1$) by ice ($K_a = 3$–4). Moreover, they measured K_a at negative temperatures in fine-grained soils (clay loam, silt loam), showing that the VWC for ice-water mixtures was within (±2.5%) of values calculated by Topp et

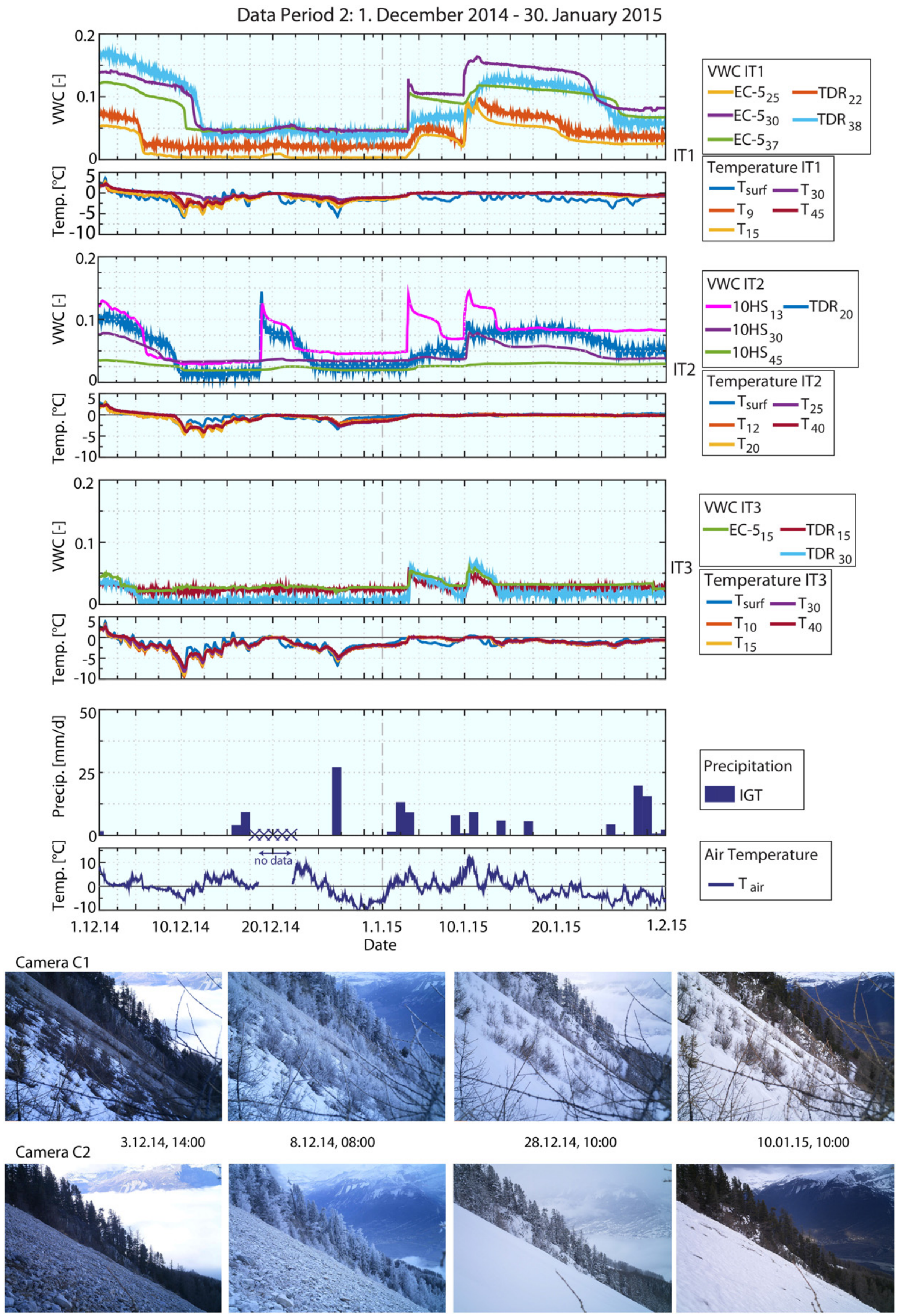

Fig. 8. VWC, temperature and precipitation at IT1–IT3 from 1st December 2014 to 31st January 2015. The ambient air temperature recorded at the IGT weather station is shown below the other graphs. The sub-index in the legend indicates the sensor depth in cm. Missing data are marked with crosses. Photos from selected dates (cameras C1 and C2; Fig. 1) are shown on the bottom.

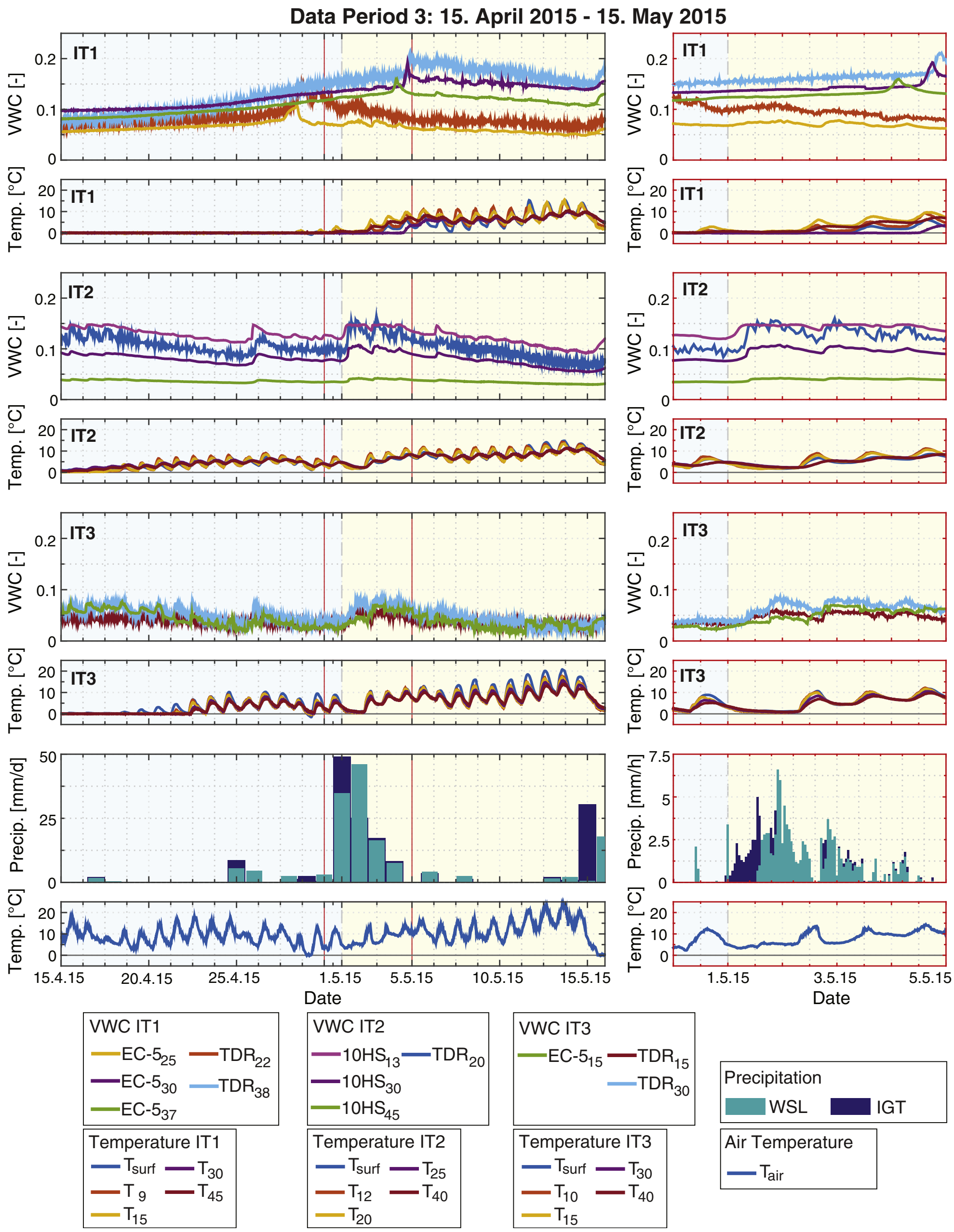

Fig. 9. VWC, temperature and precipitation at IT1–IT3 from 15th April 2015 to 15th May 2015 on the left hand side and from 30th April 2015 to 5th May 2015 on the right hand side. The ambient air temperature recorded at the IGT weather station is shown on the bottom. The sub-index in the legend indicates the sensor depth in cm. Corresponding photographs is shown in Fig. 10.

al.'s (1980) equation, suggesting that it could be applicable, at least, to unfrozen and frozen fine-grained soils.

Considering Patterson's approach, with Topp's values of VWC compared to soil-specific calibration, and VWCs measured at sub-zero temperatures by capacitance and TDR sensors at different depths (Fig. 8):

- IT1 TDR$_{22}$ and EC-5$_{25}$ show similar ranges of VWC, with EC-5 slightly lower,
- TDR$_{38}$ and EC-5$_{37}$ match well,
- as do IT2 TDR$_{20}$, 10HS$_{13}$ and IT3 TDR$_{15}$ and EC-5$_{15}$.

This issue has been further studied by Spaans and Baker (1995), who proposed improving VWC estimation by calibrating TDR sensors in frozen soil, dependent on VWC and temperature.

Frost heave causes change in structure and expansion of saturated fine-grained soils through ice lens formation in the frozen zone under sub-zero temperatures, accompanied by water migration from the unfrozen zone to the ice lenses (Miller, 1973; Taber, 1929; Taber, 1930). As thermodynamic equilibrium is required at the interface of the ice lens and the water, suction builds up, changing the VWC and therefore the hydraulic conductivity of the soil. Furthermore, frost heave in a steep slope can contribute to surficial movement, with surface debris rolling downslope (Matsuoka, 1998). This process is unlikely to have happened at the study site, even when soil reached sub-zero temperatures (Figs. 5, 8), although there would have been more likelihood to occur, very locally in silty soil around roots of stunted vegetation in IT1 and IT4, due to the higher content (around 10%) of fines (Fig. 3, Table 1).

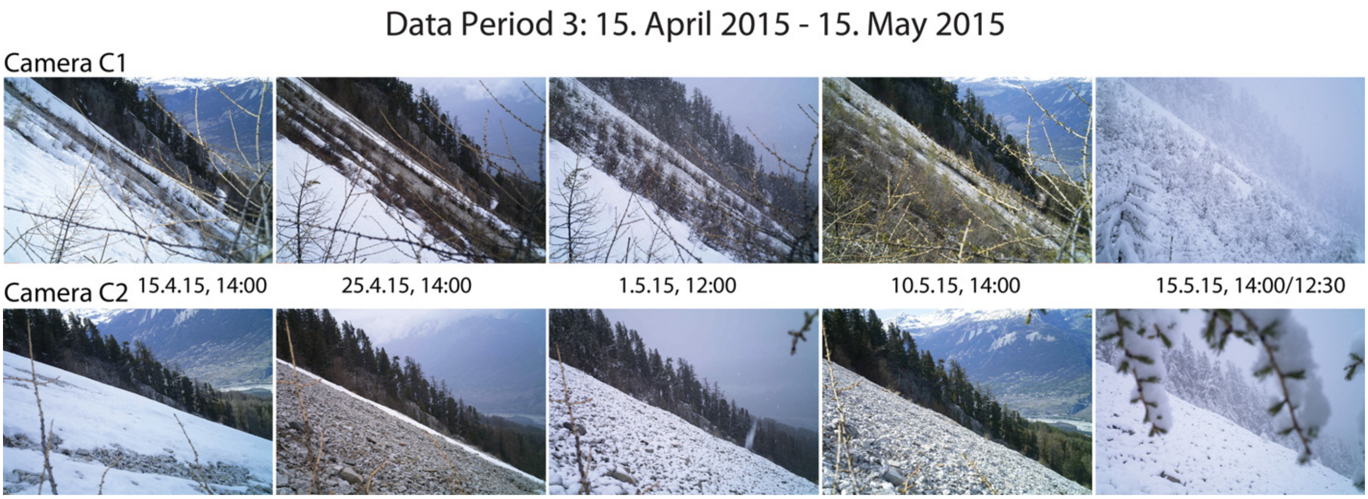

Fig. 10. Photographs from cameras C1 and C2, illustrating the time series in Fig. 9.

3.2.3. Spring/autumn

The spring snow-melt (Bayard et al., 2004) happens over conditions of sun exposure and higher temperatures during the day, producing a significant steady supply of water with more gradual infiltration. In combination with precipitation in the form of rainfall, water infiltrates through the partial insulation (e.g., remaining snow patches) into the ground, raising the VWC (Figs. 9, 10). The decrease of temperatures in autumn set the conditions for snowfall and potential soil freezing, which results in reduced VWCs.

Fig. 9 shows data from mid-April to mid-May 2015, including a larger scale plot of the most extreme precipitation event (2nd May 2015). The spring season shows the transition in soil temperature rising from minimum values, while the air temperature is already positive, with a daily variation of ~10 °C. The temperatures rise earlier in IT2 and IT3 (upslope) respectively, whereas IT1 (downslope) follows days later, confirming the effect of sun exposure. The daily temperature variation in IT1 through IT3 is greater for shallower depths (15–20 cm; yellow), compared with deeper sensors (40–

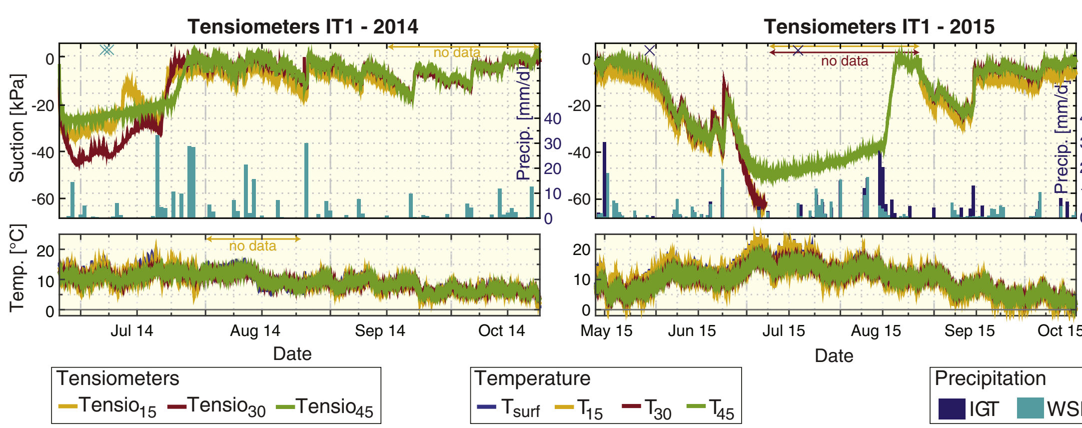

Fig. 11. Tensiometer measurements at IT1, temperature and precipitation data for two summer seasons (25th June 2014 to 23rd October 2014 and 13th May 2015 to 18th October 2015).

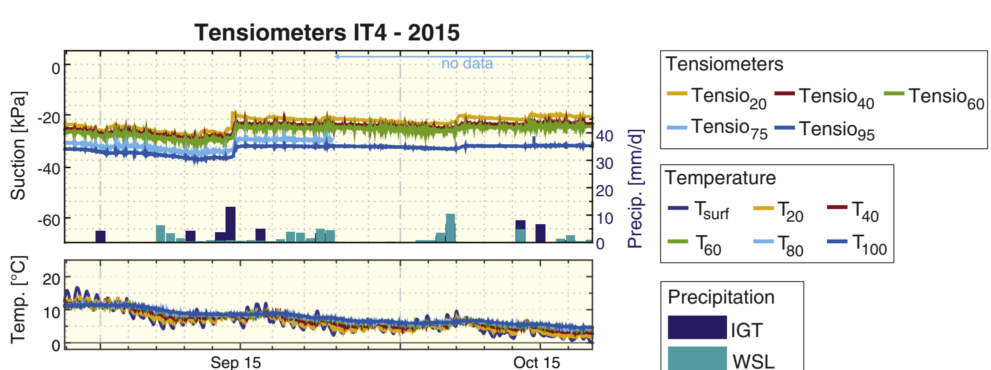

Fig. 12. Tensiometer measurements at IT4: suction, precipitation and temperature data (28th August 2015 to 20th October 2015).

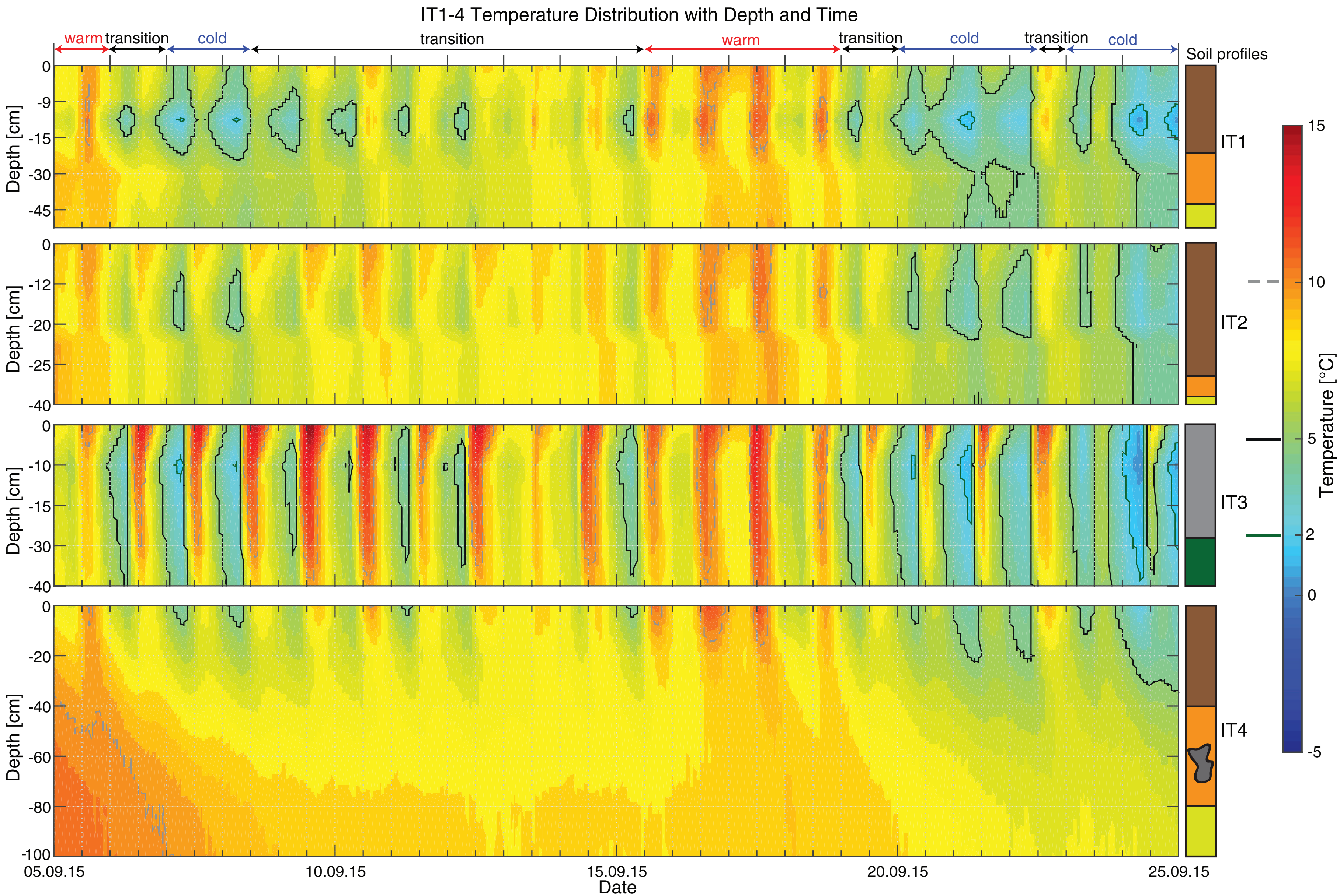

Fig. 13. Temperature distribution with depth in September 2015. IT1–IT4 are shown from top to bottom with sensor depths labelled for each trench. Contour lines are drawn at 10 °C, 5 °C and 2 °C.

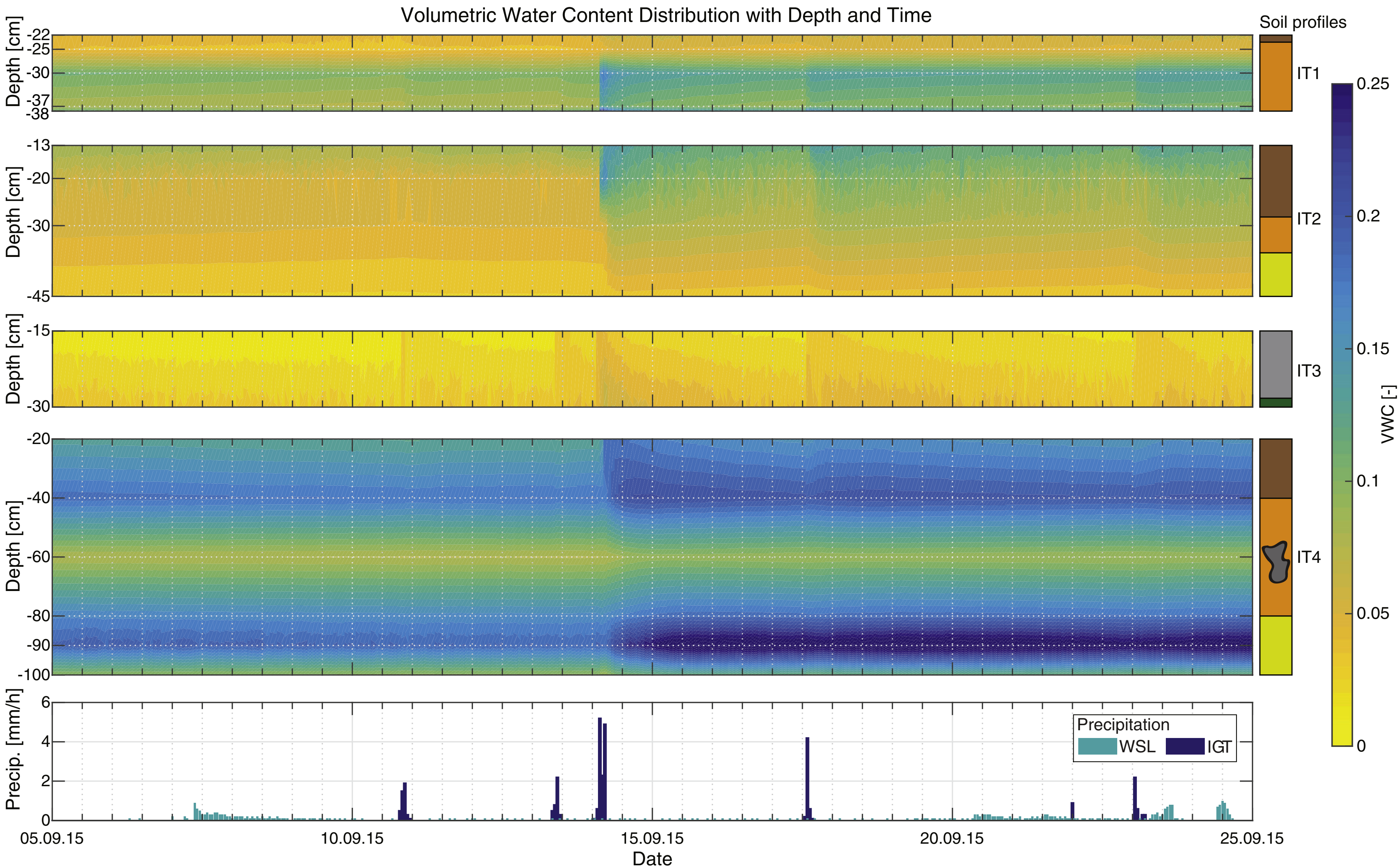

Fig. 14. Volumetric water content (VWC) distribution with depth in September 2015. IT1–IT4 are shown from top to bottom with sensor depths labelled for each trench and scaled according to the depth range of the sensors. Precipitation from both weather stations is depicted at the bottom in mm per hour.

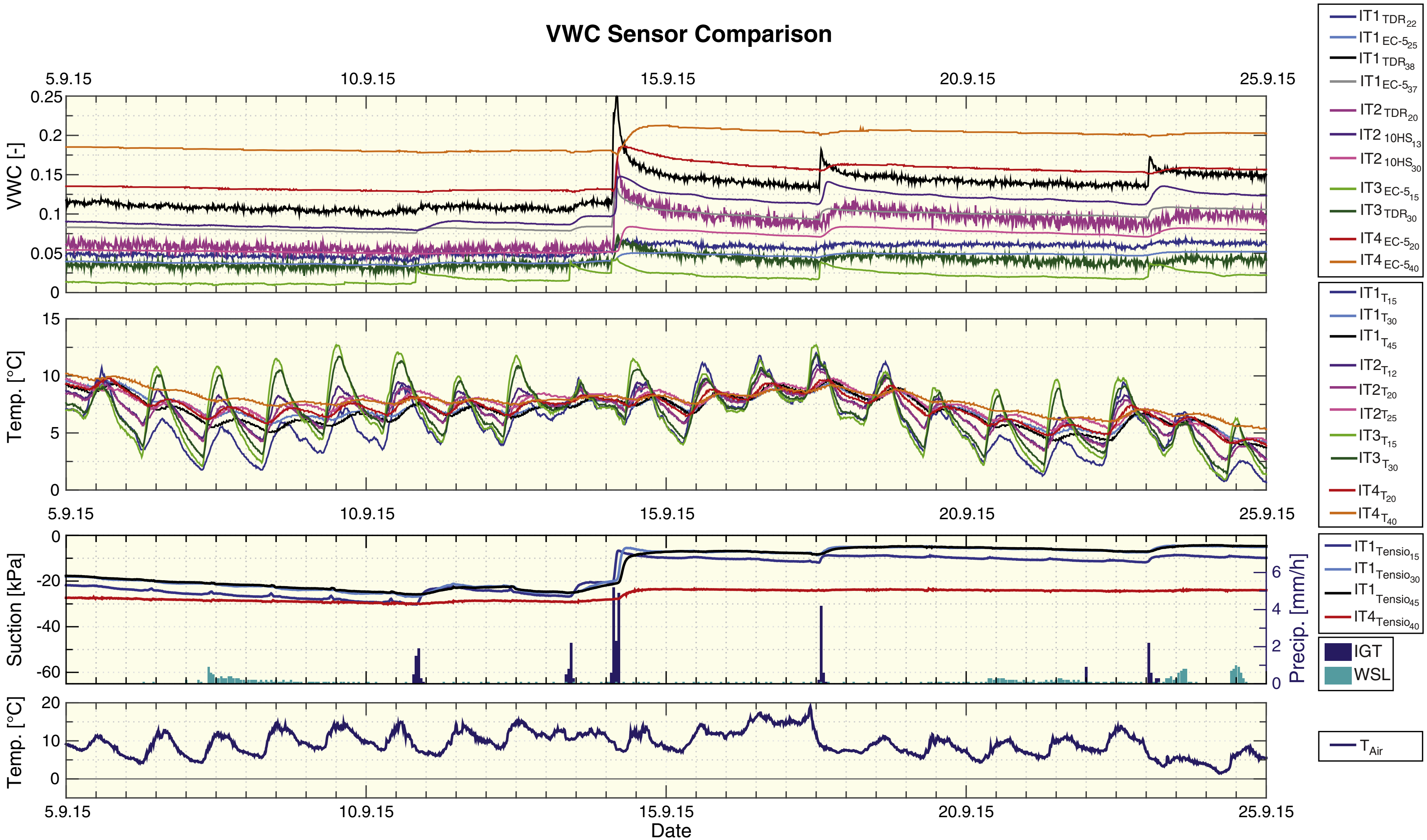

Fig. 15. Comparison between TDRs and dielectric permittivity sensors for IT1–IT4 at similar depths. From top to bottom: VWC, temperatures, suction and precipitation, and ambient air temperature in a period from 5th to 25th September 2015.

45 cm; red). However, the magnitude of this variation in IT3 is much greater at depth than in any other trench. (For interpretation of the references to colour in this figure legend, the reader is referred to the web version of this article.)

3.3. Tensiometers

The suction versus time was monitored at depth ranges equivalent to VWC measurements for IT1 and IT4 (Figs. 11 and 12). The data are

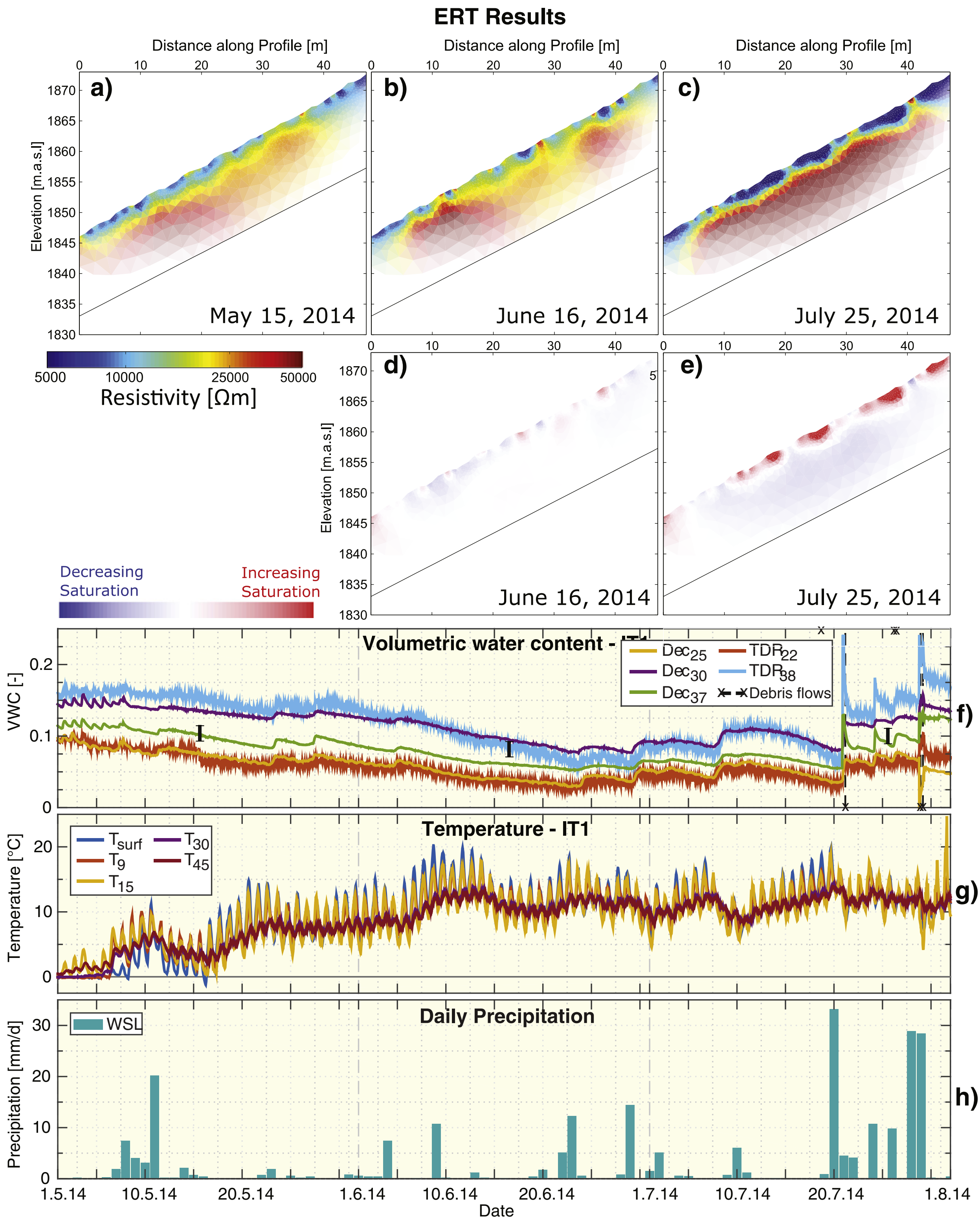

Fig. 16. a–c: Geoelectrical tomograms from 15th May, 16th June and 25th July 2014. The resistivity scale beneath the tomograms is the same for every acquisition. d–e: increasing and decreasing saturation, relative to the subsurface model obtained on 15th May (see Eq. A1 in Supplementary material A for further information). Finally, the three acquisition dates are indicated as vertical error bars within the volumetric water content measurements from TDR and capacitance sensor instrumentation in IT1 (f), which is shown from 1st May to 1st August 2014. The temperature (g) and the precipitation (h; in mm per day) are shown in the lower two time series plots.

Table 4
Comparison of VWCs from ERT to VWCs from TDRs and capacitance sensors (Dec) in IT1. "No." refers to the number of readings taken by the moisture sensors during the recording of the ERT, as VWC_{TDR} and VWC_{Dec} are averaged over all measurements. ρ is the electrical resistivity measured by ERT.

Date	No.	Temperature [°C]	VWC_{TDR} [−]	VWC_{Dec} [−]	ρ_{ERT} [Ωm]	VWC_{ERT} [−][a], m = 1.3; n = 2	VWC_{ERT} [−][b], m = 1.05; n = 1.75	VWC_{ERT} [−][b], m = 1.5; n = 1.3
15.5.2014	3	4.8	0.11	0.11	7217.9	0.14 ∓ 0.01	0.11 ∓ 0.01	0.11 ∓ 0.01
16.6.2014	4	11.7	0.06	0.07	9003.4	0.11 ∓ 0.01	0.08 ∓ 0.01	0.07 ∓ 0.01
25.7.2014	4	12.1	0.1	0.1	5363.7	0.14 ∓ 0.02	0.10∓ 0.01	0.10∓ 0.01

[a] *m* and *n* taken from literature (e.g. Archie, 1942; Lowrie, 2007; Schön, 1983).
[b] *m* and *n* calibrated using the first measurement (15th May 2014), then used in subsequent calculations of VWC_{ERT}.

plotted to a monthly scale, separated by dashed lines, corresponding to the different periods. Missing or excluded data were marked by a continuous solid arrow at the top of each graph, using the colour trace for the malfunctioning sensor.

Fig. 11 shows the suction measured in IT1 at 15, 30 and 45 cm depth, complemented by daily total precipitation in mm/day, plotted on a parallel y-axis and temperatures at different depths in a separate plot below. Periods run from the end of June to October 2014 and May to October 2015.

The three tensiometers at IT1 were installed in soil units, A, B, and C, (roots with gravel and fines, gravel with sand and fines, and coarser gravel respectively, GP-GM, Section 2.1). Correlation between the loss in suction after rainfall events can clearly be observed, after all tensiometers show a significant increase in pore water pressure during periods of high precipitation in July 2014. In addition, shallower tensiometers react faster after a rainfall event than the deeper tensiometers, due to top-down infiltration.

The unsaturated hydraulic conductivity of the soil will decrease during July 2014 and 2015 (maximum annual temperatures) due to the higher suction level, resulting in a small variation of the suction, regardless of the rain events recorded. The soil only approaches saturation after a major rainfall event, leading to higher permeability and a more dynamic response to rain infiltration.

Fig. 12 shows the suction measured in IT4 (GP-GM) at five depths (20–95 cm), complemented by daily total precipitation and temperatures. The period extends from the end of August to October 2015. Suctions increase with depth, indicating top-down infiltration through macro-voids after rain (September 15th), with gradual recovery of suction, which is surprising given the lenses of coarser gravel exposed in IT4 (Fig. 2).

3.4. Temperature and VWC with depth

Fig. 13 shows the temperature distribution with depth from 5th to 25th September 2015 for IT1–IT4, from top to bottom, respectively. The temperatures are indicated by colours (blue for colder, red for warmer), displayed in a colour bar on the right hand side. Dashed and solid (black and green) contour lines represent the boundaries at 10 °C, 5 °C and 2 °C respectively. Each depth label corresponds to a depth where sensors are located. The maximum plot depth represents the deepest sensor in each trench, ranging from 40 (IT2–IT3) to 100 cm (IT4). This 20-day autumn period (Fig. 5) is characterised by a

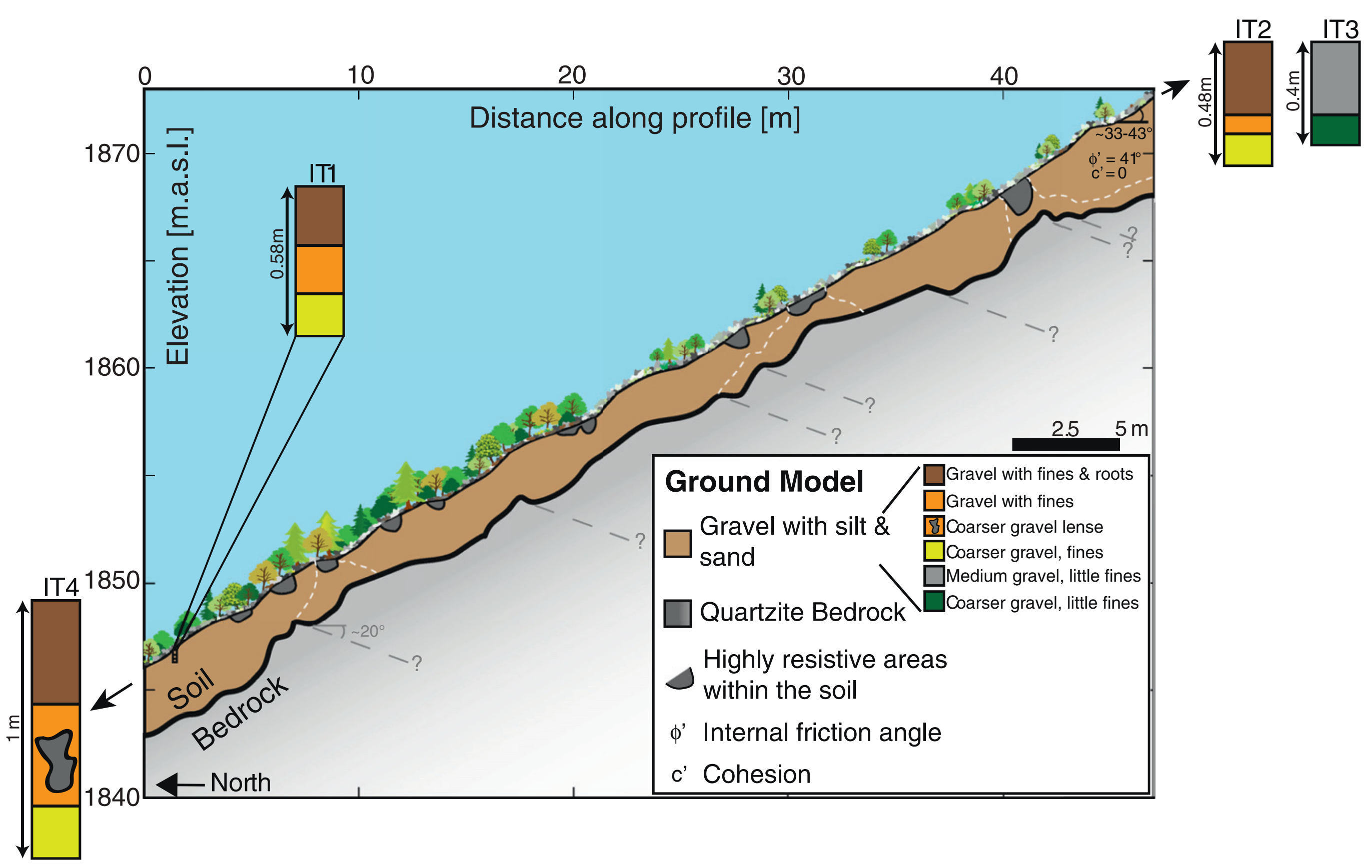

Fig. 17. Ground model derived from ERT measurements on profile 1. A visual description of the soil observed in IT1–IT4 is included, as well as some of the most important parameters, such as the friction angle.

Table 5
Geotechnical soil parameters used in the ground model.

Section	Classification (SN 670004-2b NA)	Percentage of fines [%]	Friction angle, critical state ϕ' [°]	Cohesion [kN/m^2]	G_s [−]
Downslope	GP-GM	5–10	41	0	2.68
Upslope	GW-GM	0–5	41	0	2.68

decreasing trend in temperatures, with fluctuations between 1 and 13 °C, while the volumetric water content responds dynamically to rain precipitation. Periods of warmer, colder and transition temperatures can be identified in the soil in IT1 (Fig. 13), showing a significant response of the soil to variations in ambient air temperature, even though the general trend is decreasing.

Reddish or blueish vertical 'strips' alternate daily. The response is more apparent at shallower depths (<20–25 cm) corresponding to GP-GM soils (Table 1), with nearby e = 0.52 (D1, Table 2, Fig. 1), the influence is less and temperatures lag behind in deeper, generally coarser, soil. The temperatures during warm and cold periods are about 7–13 °C and 1–5 °C, respectively with transition zones of 3–7 °C. The temperatures plotted as ground level (0 cm depth) correspond to a sensor installed in the data logger, situated on the surface a few metres from the trench and can be warmer than the temperatures measured in the soil particularly for the cold and transition times. The lowest daily temperatures over all trenches were recorded at 12 cm depth at IT1.

The soil temperatures are generally warmer in IT2 than IT1, because the soil is coarser (GW; Table 1), albeit with a similar e = 0.51 (D3, Table 2, Fig. 1). As in IT1, the influence of ambient air temperatures extends to the trench bottom, with greater variation in the top 25 cm. Periods of transition and cold are less evident due to greater thermal conductivity; this can be related to less vegetation and greater sun exposure than for IT1 (Fig. 1), warmer periods are similar in both trenches. Ambient temperature variations in IT3 affect all depths at the same time. Heat is transferred into the soil more immediately and uniformly than for other trenches, due to coarser (GW, Table 1) more permeable soil (Fig. 2c), and higher e = 0.66 (D4, Table 2). Greater sun exposure (Fig. 1) with generally lower values of VWC (Fig. 5), contribute to these greater daily variations in soil temperature, with temperatures of 12 °C and significant drops to 2 °C over 24 h (Fig. 13, 7–9th July).

Poorly graded gravel (GP-GM) in IT4, with a similar content of fines to IT1 (Table 1), less vegetation and e = 0.58 measured nearby (D2, Table 2), could explain the higher temperatures during cold and transition periods than for IT1 at similar depths. Soil temperatures exhibit daily variations until depths of 40 cm, whereas sensors below this depth are less influenced; they exhibit a gradual transition to a colder season instead, with particularly cold trends noticeable between 5–13th and 18–23rd, starting at depths of 10 cm to the trench bottom (Fig. 13).

Fig. 14 shows the VWC distribution with depth for the same time period as for Fig. 13, for IT1–IT4 from top to bottom, respectively. Colours ranging from yellow to blue (colour bar on the right hand side) represent increasing VWC. Each depth label corresponds to the depth where sensors are located. Maximum depths vary from 30 (IT3) to 100 cm (IT4) and the plots are scaled accordingly.

This VWC representation enhances the understanding of water infiltration into the soil. Precipitation events are clearly observable as 'wet fronts' in each of the trenches (e.g. on 14th September 2015). IT1 shows lower VWCs (0.05) over the top 28 cm and higher VWCs (0.1–0.2) below, during all periods of observation, with an increase during the rain event (14th September) to 0.015, when 4 h of rain intensity (1–5 mm/h) occurred. Since there is no visible sign of water infiltration and pore water pressure dissipation into the shallow depths, it is possible that lateral flow occurred in the scree slope through the coarser soil layer.

In all other trenches, water infiltrates during significant rainfall events, increasing the VWC to different degrees and depths. Drainage occurred from the top 30 cm in IT2 into the coarser underlying gravel. The narrowest range and lowest VWCs are exhibited in IT3, due to fast infiltration and dissipation of pore water pressure from the much coarser material, with exponentially decaying trends after each rain event (14th, 17th and 23rd September).

Higher VWCs and drainage at 60 cm depth into a coarser gravel layer typify data from IT4, located nearby IT1 (Fig. 1). While a significant increase in saturation was observed in a 10 cm thick layer (depths of 0.9–1 m) after 15th September, and maintained for at least 10 days until the end of the period (25th September), the tensiometers above and below this layer (Tensio75, Tensio95; Fig. 12) maintained suctions of between 30 and 40 kPa. This can be interpreted as pore water pressure build-up in a potential failure surface.

3.5. Sensor comparison: TDR vs. capacitance sensors

Fig. 15 shows the comparison between TDRs and capacitance sensors (EC-5, 10HS) at similar depths, which is complemented by measurements of temperature, suction, precipitation, soil and ambient air temperature. All VWC sensors consistently measure within a range of 0 to 0.3, which is expected, considering the given range of porosity (Sections 2.2 and 2.6). Resulting time series from capacitance sensors and TDRs generally exhibit a similar dynamic response in terms of VWC to rain infiltration.

Sensors at similar depths in the same trench, or similar depths in different locations, agree in terms of peak occurrence, but not in magnitude of variation, nor in increase and decay patterns.

Comparing sensors TDR_{38} and EC-5_{37} in IT1, the response on 14th September is immediate in both cases with a significant, sharp peak, and drainage in the coarser gravel represented by concave decay pattern due to high hydraulic conductivity. However, the magnitude of variation in VWC for the TDR is greater than for the EC-5. This can be attributed mostly to the heterogeneity of the soil, the volume of sensitivity, because the EC-5 averages the VWC over a larger volume than the TDR and possibly to the dependency of the EC-5 sensors on temperature (Section 2.4.1.2). Even though, the daily temperature variation recorded at IT1 in T_{30} and T_{45} on 14th is actually smaller than in IT3 and other sensors in IT1 at shallower depths, the trend in temperatures varies between 4 and 8 °C during these two weeks. When comparing the rain events on 17th and 23rd for the same sensors, the difference in variation of magnitude of VWC is less, but the patterns of decay in VWC change after rainfall. Sharp peaks develop with a concave decay profile (IT1, TDR_{38}) in contrast to softer shape peaks and convex decays (IT1, EC-5_{37}), that can be explained by the soil heterogeneity or a larger volume of sensitivity for the capacitance sensors. Two other sensors TDR_{22} and EC-5_{25} in IT1 at similar depth, show similar values of VWC and variations in VWC after a rain event, with slightly higher VWC recorded at TDR than EC-5 sensors, for the reasons explained before.

Capacitance sensors $10HS_{13}$ and $10HS_{30}$ and TDR_{20}, located at different depths in IT2, reaction times were compared as a reference. The sensors have similar reaction, with a slight lag from $10HS_{30}$ on 14th September (also observed for deeper sensors in other trenches), due to the initial smaller rain intensity (mm/h) (Fig. 15) that probably infiltrated only to shallower depths. $10HS_{30}$ and TDR_{20} registered similar VWCs before the rain, with greater magnitude response for TDR_{20}, which remains at a higher VWC after that. Sensors installed nearby at the same reference depth (Fig. 1) $10HS_{30}$ (IT2) and TDR_{30} (IT3) were also compared. Both sensors indicate similarly low VWCs (GW, Table 1), and VWC in TDR_{30} (IT3, e = 0.66) is lower than $10HS_{30}$ (IT2, e = 0.51), as would be expected. Mittelbach et al. (2011) also compared

TDR and 10HS in clayey loam, and have preferred 10HS in medium to low VWC using site-specific calibration, because of the greater sensitivity and accuracy in this specific range.

Finally, corrections for temperature effects could be applied to account for some of the differences, whereas the remaining discrepancies can be due to laboratory calibration, imperfect installation, varying volumes of influence as well as the heterogeneity of the gravelly soil.

3.6. Electrical resistivity tomography (ERT)

The resulting geoelectrical tomograms in Fig. 16a–c show the subsurface resistivities obtained from inversion of the ERT data acquired on 15th May, 16th June and 25th July 2014. All models depict a two-layered subsurface: an upper, relatively low resistive layer, which can be attributed to the unsaturated gravelly soil and a highly resistive layer underneath, which is assumed to represent the quartzite bedrock.

The precipitation data before each of the acquisitions show that the conditions were relatively dry and undergoing a drainage phase for the first two campaigns, whereas the data acquired in July was recorded within a period of heavy rainfalls.

These seasonal variations are mostly reflected in resistivity changes within the soil layer, in particular as a significant reduction of resistivities in the July model. The saturation relative to the subsurface model obtained in May (Fig. 16d–e) clearly reflects these conditions; there is a slight net near-surface decrease in saturation in June, whereas an increase in saturation is observed within the soil layer in July. This trend in near-surface soil saturation corresponds very well to the volumetric water content measurements (which are directly proportional to saturation; (Eq. (1)) from TDR and dielectric permittivity sensors installed at shallow depths within IT1.

Numeric VWC values calculated from resistivity measurements using Archie's law (Eq. (1)) are presented in Table 4. It should be noted, that values for VWC_{ERT} were calculated using different cementation factors m and coefficient of saturation n. For all calculations, the resulting VWC_{ERT} agree very well with the saturation trend and the magnitude measured by either type of moisture sensor: higher VWC values in May, lower values (relative decrease in saturation of the gravelly soil) during the dry period in June to higher values again during the period of heavy rainfalls (relative increase in the saturation of the soil) in July 2014. However, the VWC_{ERT} were systematically overestimated when using literature values for m and n. Determining m and n by matching the VWCs from the first acquisition (15th May 2014) and using them in subsequent calculations, a very good fit of the VWC_{ERT} to the VWC_{TDR} and the VWC_{Dec} was found for all of the acquisition dates.

Two pairs of m and n achieved this fit very well but even though estimation without soil specific laboratory measurements is difficult, $m = 1.5$ and $n = 1.3$ was discarded, because an increase in the cementation factor (from the literature value of 1.3 estimated for loose materials) would mean an increase in cementation, which is certainly not the case in this gravelly scree. Hence, the VWC_{ERT} are indicated as vertical error bars in Fig. 16f, using the VWC_{ERT} calculated with $m = 1.05$ and $n = 1.75$. The resulting VWC_{ERT} fit best with the VWCs from the dielectric permittivity sensor at 37 cm and the TDR at 38 cm depth. The remaining differences (to other sensors) were most likely due to the following factors:

- both methodologies of ‘measuring’ the VWC are indirect;
- tomograms consist of model cells larger than the cylinders of influence of individual moisture sensors in IT1 and hence an average (spatial) resistivity of surrounding cells was calculated for the comparison. In addition, the VWCs from TDR and dielectric permittivity sensors (Table 4) are also (temporal) averages, calculated over the duration of the ERT acquisition;
- parameters used in Archie's law, such as the resistivity of the pore water and the porosity, were only inferred from preliminary measurements.
- the ERT profile 1 is representative of the specific area of measurement in IT1, but the heterogeneity of the soil has to be taken into account, when comparing recorded VWCs, because of the slight difference in location (Fig. 1).

3.7. Slope characteristics

3.7.1. Sections of the slope

The variation of VWC by type of moisture sensor versus time and depth, within all of the trenches IT1–IT4, is shown in Figs. 5, 14 and 15. The range of VWC recorded at IT2 and IT3, compared to IT1 and IT4, is remarkably narrow for the dielectric permittivity sensors as well as the TDR measurements. These differences in the range of VWC, in addition to the VWC and temperature trends observed, support splitting the slope into up- and down-slope sections, with the following characteristics:

3.7.1.1. Upper scree slope (upslope).

Volumetric water content:

- low range of VWC (e.g. IT2/IT3), Fig. 5;
- Faster infiltration and drainage of water due to predominance of coarser soil with less fines. (e.g. IT3), Section 3.4, Fig. 14;

Temperature:

- temperatures can rise earlier (by up to half a month) than in downslope locations, due to greater sun exposure, Fig. 5;
- daily variations are higher and more pronounced for all sensor depths (e.g. IT3), Section 3.4, Fig. 13;
- extreme maximum values during winter and summer respectively (IT3) due to a coarser soil with higher permeability, Fig. 5;
- earlier snow-melt caused by greater sun exposure (IT2/IT3).

3.7.1.2. Lower scree slope (downslope).

Volumetric water content:

- higher range of VWC (e.g. IT1/IT4), Figs. 5, 14;
- VWC can rise due to infiltration and possible lateral flow of water downslope (IT1/IT4) Section 3.4, Fig. 14;

Temperature:

- more insulation and less sun exposure due to patches of vegetation, Figs. 1, 5;
- daily variations influenced by ambient air temperature are greater than upslope in the first 20–30 cm and less pronounced for deeper sensors (e.g. IT1/IT4), Section 3.4, Fig. 13.

3.7.2. Ground model

The ground model in Fig. 17 (with parameters in Table 5) was derived from the ERT tomograms (hence showing only the lower part of the scree slope). The boundary between the upper soil layer and the highly resistive bedrock underneath can be seen on each of the recorded tomograms (Fig. 16), however, it is clearest in the results obtained from the recordings on 25th July 2014. This measurement took place at the end of a rainy period and therefore current injected into the ground could penetrate more effectively and deeper into the saturated (more conductive) ground. Hence, the solid black line could be drawn in the ground model to divide the two layers.

All ERT surveys, but in particular those that were carried out during dry periods (e.g. 16th June 2014), reveal (local) areas of high resistivity near the surface. Most of these were not consistently observed at the same spots along the profile, were limited in size and could be explained by the difficult ground coupling of an electrode in a dry and highly resistive soil in the respective area. A few of these “patches” were more extensive than others, and could be interpreted to extend down to the bedrock (marked with dashed, light grey lines in the ground model). These were particularly visible on the tomogram from 25th July.

However, field observations, as well as GPR measurements on the lower part of the slope, indicate that it is rather unlikely that the bedrock rises to the surface. Furthermore, geological observations favour a series of "steps" at the soil-bedrock interface below ground, as nearby bedrock outcrops above ground exhibit rock layers inclined southward (into the slope) with 10–30° (see also Gabus et al., 2008a, 2008b). Assumed bedrock layers are therefore indicated in the ground model with dashed grey lines.

The highly resistive patches on the upper part of the profile, where there is less vegetation (mostly small trees, bushes and shrubs), can be explained as large boulders (estimated up to 0.5 m in diameter), which have been deposited on the surface and which also made electrode insertion difficult. Such boulders are not connected to the bedrock, but might produce a more extensive area of high resistivity. In addition, lenses consisting of larger cobbles, and even boulders, have been discovered within finer gravelly soil, e.g. during the excavation of IT4 (Fig. 2). Such lenses could also be attributed to highly resistive areas.

Due to the shallow depth of the bedrock (1–3 m), it is very difficult to determine resistivity changes within the soil layer. Subtle differences in grain size distributions were seen from trench and soil excavations (Figs. 2 and 3). Although these volumes are too small to be detected by ERT measurements (with an electrode spacing of 1 m), the soil is therefore depicted in the ground model as a uniform layer of gravel with sand and silt. However, a schematic description of the soil profiles in the trenches has been integrated as well, even though only IT1 is located along the ERT profile used for the ground model.

A friction angle of 41° was obtained using a constant shear drained triaxial stress path tests (CSD). A series of CSD triaxial tests were carried out in a medium (150 mm diameter) and large (250 mm diameter) scale apparatus using reconstituted specimens (for further information, see Grob, 2015).

4. Conclusions

Combining geotechnical and geophysical techniques has led to greater insight about the characteristics of a steep alpine scree slope. A ground model that estimates soil thickness and depth to bedrock, strength parameters, and soil classification, can be used in a posterior analysis of slope response to environmental perturbations through physical and/or numerical modelling. Furthermore, natural hazards can be assessed more effectively to provide input to needs for early warning systems and any mitigation measures.

Long-term monitoring and extensive characterisation using instrumented trenches, geophysical surveys, meteorological data and photographic observation of the slope surface yielded complementary and therefore well integrable results and gave useful indications of processes that could cause three prevalent types of downslope movement and changed perceptions of the most likely events.

Initially, it had been hypothesised that the most likely failure mechanism would be through shallow landslides, triggered by rainfall infiltration and lateral flow in a saturating soil that is heterogeneous in terms of porosity and grading. Given that the slope angle was between 33 and 43° and the friction angle is 41°, there remains some potential for small slips to occur if pore water pressures become positive over a significant layer that runs more or less parallel to the surface (as observed in 1 m depth in one of the trenches). However, the greatest number of downslope movements arise either from boulders falling and toppling downslope, being deposited temporarily in metastable positions, and remobilised either by repeated cycles of freezing and thawing, and snow-melting processes in winter or eroded by rainfall and runoff during the rest of the year.

Seasonal, daily and event driven patterns in changes of VWC, temperature and suction could be identified during the two years of monitoring and there is an agreement in trends of the VWC between dielectric permittivity sensors EC-5, 10HS and TDR in their response to rain infiltration, freezing and thawing processes. Correction factors could be applied in future for capacitance sensors (EC-5, 10HS) to allow for phase change between water and ice. Remaining differences in VWC from neighbouring devices, or similar depths, can be attributed to different installation locations and soil heterogeneity.

VWCs obtained from instrumentation were compared to values independently calculated from ERT measurements, conducted on different dates from May–July 2014. It was found that even though seasonal saturation trends agreed, VWC values were systematically overestimated by ERT, when using literature values for two parameters in Archie's law. A better fit was obtained, when these parameters were calibrated by matching one of the ERT acquisitions to the local trench measurements recorded at the same time. Hence, the agreement of VWCs from both types of measurements led to the conclusion that ERT indeed provides a convenient and fast way to infer VWC values over a larger area (spatial resolution), but has to be carefully calibrated using local VWC measurements, which in turn have the advantageous ability to more frequently record data (temporal resolution). "Small scale" trench instrumentation and "larger scale" ERT surveys complement each other very well and therefore, when combined and calibrated properly, can substantially enhance the characterization and monitoring of (steep) alpine scree slopes.

Acknowledgements

The authors are most grateful for funding from the SNF Project No. 200021_144326/1 and Canton Valais, together with the Councils of Agarn and Leuk. The project also contributes to the TRAMM2 programme of the Competence Centre of Environmental Sustainability. Furthermore, we wish to acknowledge, in particular, the support from Pascal Stoebener (WSL), Brian McArdell (WSL), Prof. Dr. Hansruedi Maurer (Exploration and Environmental Geophysics, EGG), Dr. Andrew Kos, Dipl. Ing. Ralf Herzog, Ernst Bleiker, Thomas Buchli, Reto Grob and Nicole Oggier. We would also like to thank Peter Molnar for providing us with insights regarding the recorded data series of rainfall. For the help with sensor-related problems, we would like to thank many employees of Decagon Devices.

Appendix A. Supplementary data

Supplementary data to this article can be found online at http://dx.doi.org/10.1016/j.enggeo.2016.11.018.

References

Archie, G.E., 1942. The electrical resistivity log as an aid in determining some reservoir characteristics. Trans. AIME 146 (01), 54–62.

Bayard, D., Stähli, M., Parraiaux, A., Flühler, H., 2004. The influence of seasonally frozen soil on the snowmelt runoff at two alpine sites in southern Switzerland. J. Hydrol. 309 (1), 66–84.

Beck, A., 2010. Measurement of unsarurated hydraulic conductivity with the instantaneous profile method. Semester Project ETH (Zurich, Switzerland).

Bichler, A., Bobrowsky, P., Best, M., Douma, M., Hunter, J., Calvert, T., Burns, R., 2004. Three-dimensional mapping of a landslide using a multi-geophysical approach: the Quesnel Forks landslide. Landslides 1 (1), 29–40.

Bogena, H.R., Huisman, J.A., Oberdörster, C., Vereecken, H., 2007. Evaluation of a low-cost soil water content sensor for wireless network application. J. Hydrol. 344 (1), 32–42.

Bogoslovsky, V.A., Ogilvy, A.A., 1977. Geophysical methods for the investigation of landslides. Geophysics 42 (3), 562–571.

Brunet, P., Clément, R., Bouvier, C., 2010. Monitoring soil water content and deficit using electrical resistivity tomography (ERT) — a case study in the Cevennes area France. J. Hydrol. 380 (1), 146–153.

Fankhauser, K., 2014. Geophysical Slope Characterization Using GPR and ERT in an Active Debris Flow Catchment. (Master Thesis). EEG, ETH Zurich.

Friedel, S., Thielen, A., Springman, S.M., 2006. Investigation of a slope endangered by rainfall-induced landslides using 3D resistivity tomography and geotechnical testing. J. Appl. Geophys. 60 (2), 100–114.

Gabus, J. H., Weidmann, M., Burri, M., & Sartori M. (2008a). Feuille 1287 Sierre, *Atlas Géologique de la Suisse 1:25'000, Carte 111*, swisstopo, Wabern.

Gabus, J. H., Weidmann, M., Burri, M., & Sartori M. (2008b). Feuille 1287 Sierre, *Atlas Géologique de la Suisse 1:25'000, Note expicative*, swisstopo, Wabern.

Grob, R., 2015. Measurement of Soil Properties for Gravels in a Scree Slope Using Large Scale Triaxial Testing. (Master Thesis). IGT, ETH Zurich.

Günther, T., 2011. Timelapse ERT inversion approaches and their applications. Geoelectric Monitoring, pp. 91–97.

Günther, T., Rücker, C., 2013. Boundless Electrical Resistivity Tomography — The User Tutorial (Available at: www.resistivity.net).
Günther, T., Rücker, C., Spitzer, K., 2006. Three-dimensional modelling and inversion of DC resistivity data incorporating topography — II. Inversion. Geophys. J. Int. 166 (2), 506–517.
Hack, R., 2000. Geophysics for slope instability. Surv. Geophys. 21 (4), 423–448.
Hayashi, M., 2004. Temperature-electrical conductivtiy relation of water for environmental monitoring and geophysical data inversion. Environ. Monit. Assess. 96 (1–3), 119–128.
ICT International, 2008. 10HS volumen of sensitivity. http://ictinternational.com/content/uploads/2014/03/10HS-Volume-of-Sensitivity.pdf (Accessed 23.09.16).
Lehmann, P., Gambazzi, F., Suski, B., Baron, L., Askarinejad, A., Springman, S.M., Or, D., 2013. Evolution of soil wetting patterns preceding a hydrologically induced landslide inferred from electrical resistivity survey and point measurements of volumetric water content and pore water pressure. Water Resour. Res. 49 (12), 7992–8004.
Lowrie, W., 2007. Fundamentals of Geophysics. Cambridge University Press.
Lucas, D.R., Askarinejad, A., Herzog, R., Bleiker, E., Springman, S.M., 2015. Volumetric water content determination by TDR sensors and decagons in gravelly soils. XVI European Conference on Soil Mechanics and Geotechnical Engineering (XVI ECSMGE 2015), Edinburgh, UK, 13.-17.9.2015:pp. 3565–3570. http://dx.doi.org/10.1680/ecsmge.60678.vol6.560.
Matsuoka, N., 1998. The relationship between frost heave and downslope soil movement: field measurements in the Japanese Alps. Permafr. Periglac. Process. 9 (2), 121–133.
Miller, R.D., 1973. Soil freezing in relation to pore water pressure and temperature. 1. International Conference on Permafrost, 2d, Yakutsk, Siberia, 1973. Papers.
Mittelbach, H., Casini, F., Lehner, I., Teuling, A.J., Seneviratne, S.I., 2011. Soil moisture monitoring for climate research: evaluation of a low-cost sensor in the framework of the Swiss soil moisture experiment (SwissSMEX) campaign. J. Geophys. Res. Atmos. 116 (D5).
O'Connor, K.M., Dowding, C.H., 1999. Geomeasurements by Pulsing TDR Cables and Probes. CRC Press.
Oggier, N.C., 2011. Simulierung von Murgängen mit RAMMS am Beispiel des Meretschibachs. (Master Thesis). ETH Zürich und Forschungsanstalt für Wald Schnee und Landschaft (WSL).
Onset Computer corporation. EC-5 volume of sensitivity application note. (n.d.). http://www.onsetcomp.com/files/15926-B%20EC-5%20Volume%20of%20Sensitivity.pdf (Accessed 23.09.16).
Otto, J.C., Sass, O., 2006. Comparing geophysical methods for talus slope investigations in the Turtmann valley (Swiss Alps). Geomorphology 76 (3), 257–272.
Patterson, D.E., Smith, M.W., 1981. The measurement of unfrozen water content by time domain reflectometry: results from laboratory tests. Can. Geotech. J. 18 (1), 131–144.
Rickenmann, D., Zimmermann, M., 1993. The 1987 debris flows in Switzerland documentation and analysis. Geomorphology 8 (2), 175–189.
Rücker, C., Günther, T., Spitzer, K., 2006. Three-dimensional modelling of DC resistivity data incorporating topography — I. Modelling. Geophys. J. Int. 166 (2), 495–505.
Sakaki, T., Limsuwat, A., Smits, K.M., Illangasekare, T.H., 2008. Empirical two-point α-mixing model for calibrating the ECH2O EC-5 soil moisture sensor in sands. Water Resour. Res. 44 (4).
Sass, O., 2007. Bedrock detection and talus thickness assessment in the European Alps using geophysical methods. J. Appl. Geophys. 62, 254–269.
Sass, O., Bell, R., Glade, T., 2008. Comparison of GPR, 2D-resistivity and traditional techniques for the subsurface exploration of the Aeschingen landslide, Swabian Alb (Germany). Geomorphology 93 (1–2), 89–103.
Schön, J., 1983. Petrophysik Physikalische Eigenschaften von Gesteinen und Mineralen. Akademie-Verlag, Berlin.
Spaans, E.J., Baker, J.M., 1995. Examining the use of time domain reflectometry for measuring liquid water content in frozen soil. Water Resour. Res. 31 (12), 2917–2925.
Springman, S.M., Askarinejad, A., Casini, F., Friedel, S., Kienzler, P., Teysseire, P., Thielen, A., 2012. Lessons learnt from field tests in some potentially unstable slopes in Switzerland. Acta Geogr. Slov. 1, 5–29.
Springman, S.M., Thielen, A., Kienzler, P., Friedel, S., 2013. A long-term field study for the investigation of rainfall-induced landslides. Géotechnique 63 (14), 1177–1193.
Springman, S.M., Lucas, D.R., Oggier, N.C., Kos, A., Fankhauser, K., McArdell, B., 2015. Study of the seasonal response of a scree slope and debris flow catchment in the Swiss alps. XVI European Conference on Soil Mechanics and Geotechnical Engineering (XVI ECSMGE 2015), Edinburgh, UK, 13.-17.9.2015:pp. 1897–1902. http://dx.doi.org/10.1680/ecsmge.60678.vol4.285.
Taber, S., 1929. Frost heaving. J. Geol. 428–461.
Taber, S., 1930. The mechanics of frost heaving. J. Geol. 303–317.
Take, W.A., Arnepalli, D.N., Brachman, R.W.I., Rowe, R.K., 2007. Laboratory and Field Calibration of TDR Probes for Water Content Measurement. Queen's University, GeoEngineering Centre, Kingston, Ontario, Canada.
Topp, G.C., Davis, J.L., Annan, A.P., 1980. Electromagnetic determination of soil water content: measurements in coaxial transmission lines. Water Resour. Res. 16 (3), 574–582.